Effects of Mo and B additives on hardness and the resistance of Cu-Ni alloy to wear,

corrosion and corrosive wear

by

Runfang Hou

A thesis submitted in partial fulfillment of the requirements for the degree of

Master of Science

in

Materials Engineering

Department of Chemical and Materials Engineering

University of Alberta

Abstract

Due to its corrosion resistance, conductivity, and modifiable mechanical properties, CuNi alloy has found a wide range of applications, especially in the marine environment. It is highly desired if the mechanical strength and wear resistance of CuNi alloy can reach a level comparable to that of steel. In this study, effects of Mo, B, and their combination on properties of CuNi alloy were investigated, including hardness and resistances to wear, corrosion and corrosive wear. The B and Mo added CuNi samples were made using an arc furnace and annealed at 600°C for 4 hours. The samples were characterized with SEM, optical microscopy and X-Ray diffraction techniques. Wear resistances of the samples were evaluated using a pin-on-disc tester. It was demonstrated that the Mo and B additives were effective in strengthening the CuNi alloy while retaining desired corrosion resistance. In particular, the combination of Mo and B additives was more effectively than a single additive to harden the alloy, leading to considerably increased wear resistance. The modified CuNi samples show their hardness comparable to that of normalized low carbon steel. The volume loss of the 50Cu-50Ni alloy caused by wear was reduced by 59% and 56% when tested in air and 3 wt.% NaCl solution, respectively, after 2 at.% B and 2 at.% Mo were added. Mo and B additives have demonstrated their great promise as new alloying elements to modify CuNi alloys.

KEYWORD: CuNi, hardness, wear, corrosive wear, molybdenum, boron

Preface

The study of this thesis research was supervised by Dr. Dongyang Li.

Pin-on-disc wear test, profilometer characterization, hardness test and corrosion test were done in Dr. Dongyang Li's research lab. SEM characterization was completed at the Scanning Electron Microscope Lab at the University of Alberta. XRD test was done with assistance from Zhen X. at nanoFAB. I was responsible for conducting experimental tests, analyzing data and writing the thesis.

Acknowledgements

I gratefully appreciate Dr. Dongyang Li's guidance and help during my study at the University of Alberta. I also want to thank the Department of Chemical and Materials Engineering faculty, staff, and my fellow lab members for their support and help.

I really appreciate the support and care from my families and friends.

Table of Contents

List of Tables

List of Figures

Chapter 1 Introduction and literature review

1.1 Corrosion of materials

Corrosion is the degradation of materials through chemical or electrochemical reactions when materials are exposed to the environment, such as air, water, acids, alkalis and soils [1]. The application of corrosion engineering is directly related to the use and service lifetime of products. Besides, it also influences the materials design, like the composition, crystal structures and properties. Corrosion usually accompanies with physical damage like wear. The concept of corrosion used to be limited to metals, which however, expands to other materials in the past decades. The degradation of materials refers to the loss of materials or reduction of the mechanical strength at the macroscopic level. Corrosion may cause serious damage to the steel industry, transportation, plants, equipment, energy generation and environment, which can result in huge economic costs. The estimated cost due to corrosion around the world is about US $2.5 trillion, which is equal to 3.4% of the global Gross Domestic Product in 2013 [2]. Corrosion may also result in the leaks of pipelines and containers, leading to the contamination of environment by the released oil, gas or other chemicals [3].

1.1.1 Mechanism

Corrosion processes are either chemical or electrochemical reactions. However, most of the corrosion occurs in aqueous media, where corrosion cells are formed, which is demonstrated in figure 1.1 [4]. The metal component with a more negative potential acts as the anode and the less reactive component acts as the cathode. The anode metal atoms lose electrons and may either dissolve in the solution or react with other components to form compounds, which would eventually lead to macroscopic materials loss if without proper corrosion controls. The corroding area of the anode metal expands and non-corroding area remains the same, as illustrated in figure 1.1 Fe is used here as an example of the anode reaction:

$$Fe \rightarrow Fe^{2+} + 2e$$
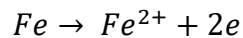
The electrons are then conducted by the metallic path connecting two electrodes to from a current flow. The cathode reactions may appear as [4]:

$$2H^+ + 2e \rightarrow H_2 \uparrow \qquad \text{in acid solution}$$

$$2H_2O + O_2 + 4e \rightarrow 4OH^- \qquad \text{in neutral or basic solution}$$

$$M^{2+} + 2e \rightarrow M \qquad \text{reduction of a metal ion}$$
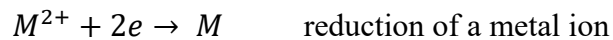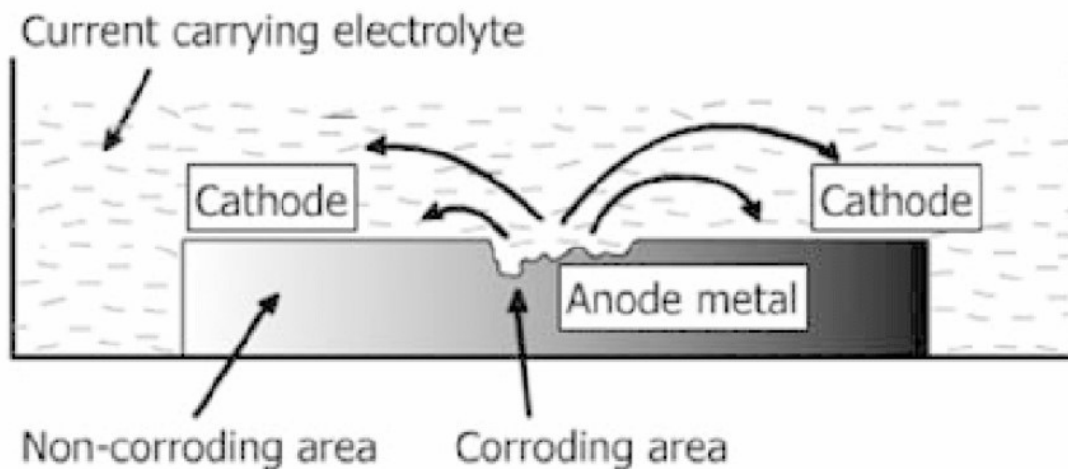
Figure 1. 1 An illustration of a corrosion cell [4]

In addition to the electrochemical corrosion, high temperature corrosion [5] happens when materials react with gas, solid or melted salts without any liquid electrolyte. It appears as a chemical process at the interfaces of the working materials and the surrounding environment. It is a serious problem for equipment working with high temperature conditions typically over 400 °C, such as heat treatment and waste incineration.

1.1.2 Types of corrosion

Based on the morphology of the corrosion product, corrosion can take place in several different forms: Uniform corrosion[6], pitting corrosion[7], crevice corrosion[8], galvanic corrosion[9], intergranular corrosion[10] and selective corrosion[11].

Uniform corrosion represents the uniform loss of materials and a very similar corrosion rate over the entire surface of the material. It is the one of the most frequent form of

corrosion to the chemical processing and manufacturing equipment. The materials'

structures appear uniform because the corrosive medium can reach every part of the

materials surface. This leads to a massive loss of materials. Thus the uniform corrosion and

its corrosion rate can usually be predicted due to its obvious corrosion behavior.

Localized corrosion, on the contrary, can be more dangerous and difficult to predict

because of the small loss of materials, which is also the majority cause of the corrosion

incident. The followings are some examples of localized corrosion.

Pitting corrosion, caused by the localized corrosion, creates small cavities over the

surface of materials. The cavities usually exhibit small dimeters on the surface but rather

large depths inside materials. As shown in figure 1.2, the pitting corrosion can be

characterized by the pitting factor, which is the ratio of the depth of the deepest cavity, p,

and the average penetration depth of the material, d.
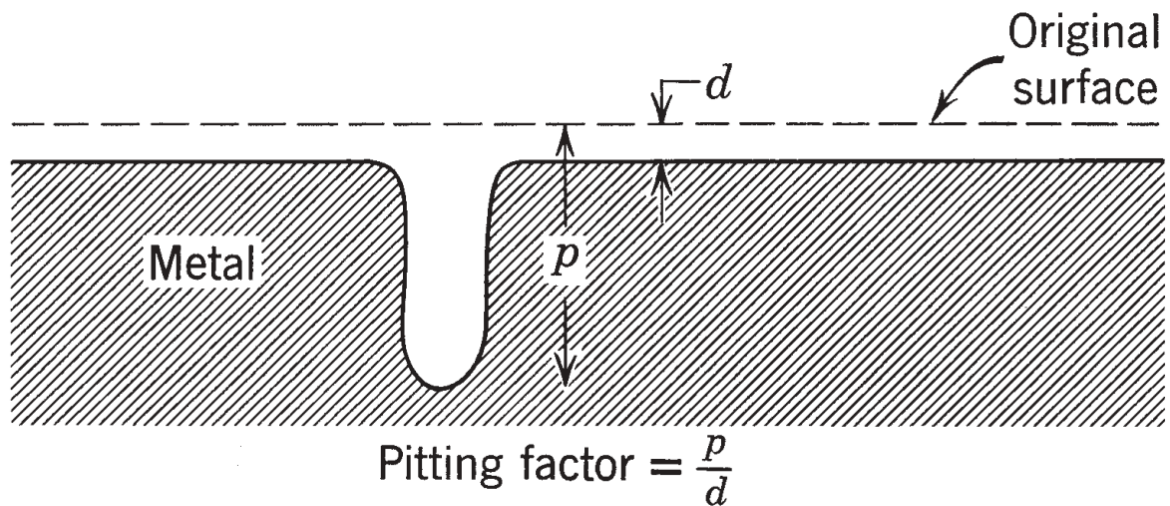
Figure 1. 2 An illustration of the pitting corrosion over the surface of a metal[1]

Crevice corrosion occurs in crevices between metal components or metal and non-metallic components. The crevices exist at the connection of different components such as threading, welding, gaskets and flanges, surface adhesion and coatings. The obstructed mass transfer of the electrolyte medium inside small gaps is the cause to this localized corrosion form. The formation of the corrosion is influenced by the crevice size and depth, materials compositions and types of electrolyte. It can happen to all metals or alloys. However, it is demonstrated that the crevice corrosion is especially common on surfaces of metals which can produce passive films to resist corrosion, such as aluminum and stainless steel.

Galvanic corrosion refers to the corrosion caused by the contact of two different types of metals in an electrolyte. The corrosion of the metal with more negative electrode potential is accelerated and the one with more positive electrode potential is protected. Galvanic corrosion is very common because of the inevitable combination of dissimilar metals to manufacture equipment. The corrosion is influenced by the potential difference of dissimilar metals, polarization condition, electrode surface area, PH, temperature, and conductivity of the electrolyte. Though the galvanic corrosion can cause damage to equipment in some situations, it can be used to protect useful equipment components by sacrificing the cheaper electrode materials with more negative potentials.

Intergranular corrosion attacks the grain boundaries instead of the bulk of grains. It is usually hard to observe this type of corrosion on a macroscopic level. However, the

mechanical strength of materials can be destroyed in a very short time. The defects, the irregular atom arrangement and possible precipitate phases at grain boundaries cause dissimilar electrochemical potentials from the bulk of grains in a corrosive medium. Thus a corrosion cell is formed with grain boundaries as anodes and grains as cathodes, which starts the corrosion.

Selective corrosion, also called as dealloying, occurs when a specific component of an alloy is attacked and dissolved in the electrolyte. It leads to the weakening of the strength and structure of the material. Dezincification of brass is a typical example of selective corrosion. Zn is usually added to Cu to enhance its mechanical strength. However, with the increase of Zn in the alloy, the dezincification becomes severe since Zn is selectively dissolved. The remaining alloy with high Cu concentration then turns to be porous and brittle.

1.1.3 Methods to control corrosion

Materials and structures design

Selecting proper materials based on materials properties and the working environment is the most effective method to prevent corrosion. Parameters influencing the selection include: cost, availability, operation conditions (types of electrolyte medium, PH, temperature, pressure), the requirement of mechanical strength, product lifetime and regulations. Besides, the design of a machine structure can be improved to prevent

corrosion. For example, these problems can be alleviated or eliminated: stress concentration, the obstruction of mass transfer, the deposition of solid particles, the formation of galvanic corrosion cell and local overheating.

Electrochemical protection

Anodic protection [12-13]

Anodic protection is used to elevate the potential of a metal surface to make it the anode of an electrochemical corrosion cell, where a protective passivation film is generated on the metal surface. The passivity due to the potentiostat protects the material in a corrosive environment. Anodic protection is commonly used for steel protection in an acid environment. Figure 1.3 demonstrates the protection of chromium-nickel steel in Sulfuric acid. Generally, an additional power supply is used to provide extra potential and current. The metal which needs to be protected is placed as an anode electrode, whose potential is increased by the power supply. When the anodic polarization is elevated to a passivation zone, a protective film is generated to protect the metal from the corrosive medium.
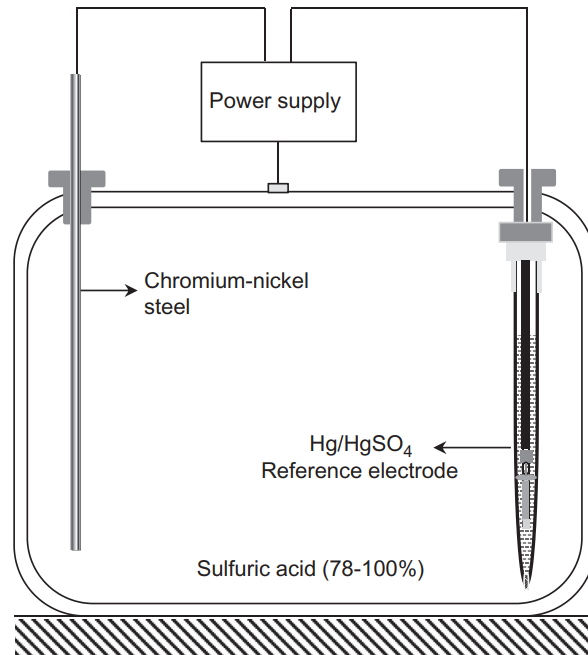
Figure 1. 3 Schematic of anodic protection to chromium-nickel steel in sulfuric acid

with the passivation film [12]

Cathodic protection [14-15]

Cathodic protection is widely used in underground and undersea equipment, such as pipelines, utility foundations and ship hulls. The cathodic potential is reduced to be more negative by an external current or potential. A more active galvanic anode can be used to protect the corrosion of cathode. For example, a zinc coating can be applied to the steel to prevent corrosion. Zinc serves as the sacrificial anode and providing electrons to the cathode, steel. The more active anode material, zinc, then sacrifices ions and degrades, which keeps the steel from corrosion. A simple cathodic protection of the electrochemical corrosion cell is illustrated in figure 1.4. The current in the metallic path is generated due

to the potential difference between two electrodes. The electrons transfer from anode to cathode, which protect the cathode from the corrosive environment.

This can also be achieved by impressed-current cathodic protection systems [16-17]. The main principle of the corrosion protection is to introduce an impressed current to induce negative polarization of the protected cathodic materials.
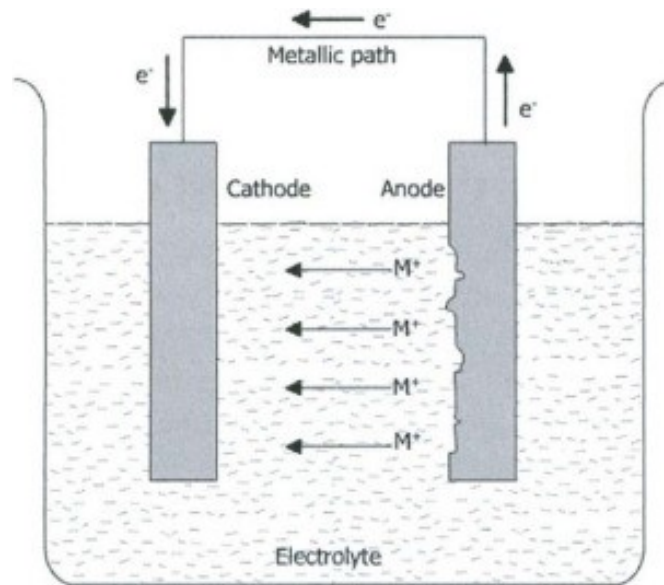
Figure 1. 4 An illustration of cathodic protection in an electrochemical cell [4]

Inhibitor protection [12]

Corrosion inhibitors are chemicals that are added to liquid or gas to prevent or alleviate the corrosion rate of metals. Inhibitor protection has advantages of convenience to use and low cost. Different mechanisms exist. Anodic inhibitors contribute to the polarization and the formation of passivation films, which increase the potential and mitigate the corrosion. Examples include chromates, molybdates, nitrites, tungstates with high oxygen content.

These anodic inhibitors react with metal ions removed from the substrate and form a new compound. The newly generated compound is then absorbed on the surface as a barrier to the corrosive medium.

Precipitation or cathodic inhibitors can react with corrosive medium and form a thick deposit layer with high electric resistance to insulate the corrosive medium from protected metals. Carbonates such as $CaCO_3$ and zinc sulfates which deposit as $Zn(OH)_2$ are widely used as precipitation inhibitors. Besides that, cathodic poisons of cathodic inhibitors, such as sulfides and bismuth, can suppress the hydrogen evolution reaction on the metal surface. Oxygen scavenger, such as hydrazine, reacts with oxygen to suppress the oxygen cathodic reaction.

Organic inhibitors which contain polar groups, form a barrier film over the surface of metals, by Van der Waals force, electrostatic attraction or chemical adsorption. Different types of chemicals include amines, imidazolines and quaternaries.

Coating

The coating generally acts as a barrier to prevent metals from the corrosive environment. Conversion coating is formed when chemicals react with the metal surface. This insoluble and protective film is then well-adhered to the metal. Common examples include phosphate coatings, chromate coatings and aluminate coatings. Besides that, sacrificial coatings are applied to steel, such as zinc-aluminum coatings. What's more, the

pore-free cathodic and continuous cathodic coatings are used to protect the substrate. Examples are noble copper coatings on steel, where an interlayer is usually applied between the coating and the substrate.

1.2 Wear

Wear is the material removal caused by dynamic contact between two surfaces, which is thus closely related to the mechanical properties of materials in contact. Although wear is a surface damage process, it can make components of machinery and facilities dysfunctional. Friction and wear are widely found in industries, such as energy production, transportation, chemical processing and manufacturing. Tribological contacts account for 23% of the global energy consumption and 3% of the energy is spent on repairing and reproducing the equipment damage from wear failure [18]. The wear failure leads to a huge economic cost of 1.4% of the global GDP every year.

1.2.1 Types of wear

Wear is due to the local failure at materials interfaces and it is influenced by many factors. Materials intrinsic properties related to the wear behavior include surface energy, microstructure, hardness, thermal conductivity and plasticity. The environment factors include temperature, medium, stress and relative velocity of contact surfaces. Wear has

different modes, including abrasive wear [19-20], adhesive wear [21-22], erosive wear [23], corrosive wear [24,25], fatigue wear [25] or fretting [26] etc.

Abrasive wear

Abrasive wear is caused by hard particles or protuberances sliding over a soft surface. These hard particles and protuberances can come from the equipment itself, the surface materials after wear damage, non-metallic abrasive such as silicon, quartz and sand. Abrasive wear can be classified into two types based on whether the hard surface is constrained or not, as illustrated in figure 1.5. Two-body wear occurs when hard protrusions, like cutting tools, rubbing another soft surface. Three-body wear refers to the situation where hard particles enter in between two soft surfaces and cause wear to either or both of the surfaces. Polishing of the metal surface by paste with small hard particles can be seen as a three-body abrasive. The wear is closely related to the hardness of particles, surface mechanical strength and microstructure.
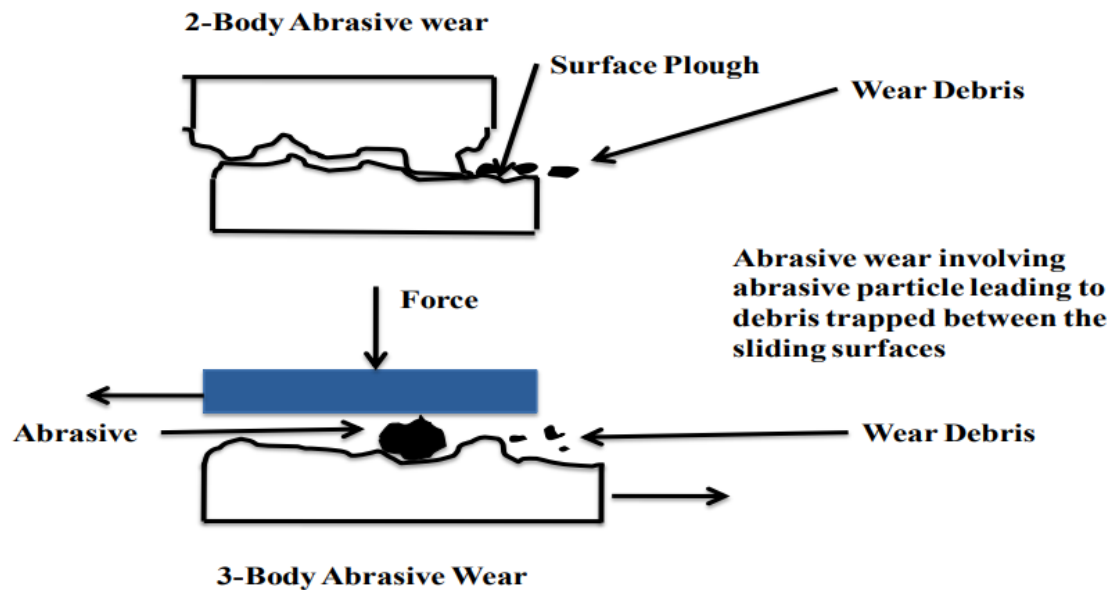
Figure 1. 5 Schematics of abrasive wear [28]

Adhesive wear

When two faces come into contact, some regions within a small area experience asperity contacts and form the adhesive junction under the extreme localized high pressure. Due to the sliding of one surface over another, this junction bond breaks and cause rupture. During this process, new adhesion continues to form and break, which leads to consecutive surface damage, as illustrated in figure 1.6. The adhesive wear generally occurs where exist a small speed of relative motion, weak contact surface oxidation films, a strong relative load and the lack of lubrication.

The materials volume loss V caused by wear is related to the load between two surfaces W, the relative sliding distance X, the hardness of the weaker surface H, and the wear

coefficient *K*. The volume loss can be calculated by

$$V = K \frac{W}{H} X$$

This equation is called Archard's wear equation. The value of *K/H* provides an indicator of the wear resistance of a system. This simple theory also indicates the proportional relationship between the wear volume loss and applied load.
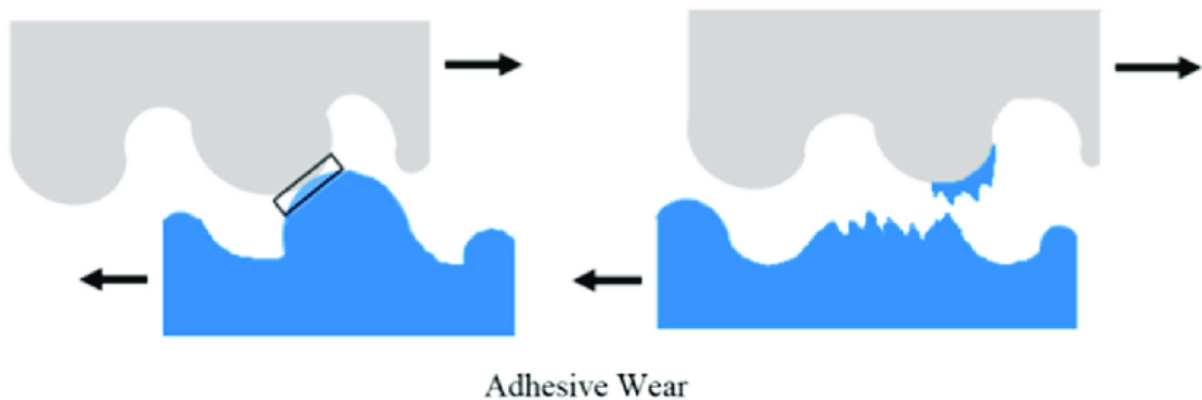
Adhesive Wear

Figure 1. 6 Schematics of adhesive wear [29]

Erosive wear

Erosive wear is the materials loss caused by impacts of hard solid particles on a surface. Based on the types of the particles and their medium, the wear has the following kinds: the impingement of solid particles, the liquid droplets, gases and cavitation of liquid medium. Erosive wear damage widely exists in nature environment and industrial production, such as the deterioration of pipelines, boiler tubes and slush pumps. However, it can also be used to improve the materials' surface properties by abrasive blasting and shot blasting. The

erosive wear is dependent on various factors, such as the surface properties and structures of the object, the speed, size, hardness and impingement angle of impact particles.

Corrosive wear

Corrosive wear can be regarded as a synergetic process of both corrosion and machinal wear. The corrosion is caused by chemical or electrochemical reactions between the frictional surfaces and their surrounding medium. Meanwhile, corrosive products are removed due to the friction and contribute to the wear as wear particles. After the previous oxidation layer from corrosion is removed, new oxidation layer forms after contacting with the medium. The corrosive wear continues with the generation of new corrosive layers and particles. Thus the loss of materials caused by corrosive wear is determined by two different processes: the growth rate of the oxidation layer and the wear rate from the relative motion. Based on the mechanism, the corrosive wear can be prevented by developing materials with a good resistance to the working environment or using a protective coating with a fixed machine operation requirement.

Fatigue wear

The continual rolling contact under stress causes the removal of localized debris of materials, which is called fatigue wear. The formation and expansion of fatigue crack come from the fact that contact shear stress is larger than the contact fatigue strength. It is very common to cyclical rolling components such as gears, rolling bearings and vehicle wheels. The stress concentration from non-metallic imperfections or metallurgical production

defects can act as the source of fatigue wear cracks, thus largely reduce the fatigue wear resistance.

1.2.2 Evaluation of wear

The wear resistance refers to the ability of a material to resist the deformation from another material in a certain gaseous or liquid medium. The performance of wear resistance is always evaluated by the loss of materials, either by the weight difference or the volume change of the sample before and after the wear test. A smaller loss of materials under the same circumstance of testing indicates a better wear resistance. Wear rate can be used to describe the wear amount per second or meter, the unit is kg/m, m^3/m, kg/s or m^3/s.

Wear testing tools

Different wear testing systems have been developed to evaluate the wear resistance of materials, as illustrated by figure 1.7 [30]. Parameters and settings can be controlled during sliding wear tests to compare wear resistances of different samples. The linear or angular speed of the disc, hardness of the abrasion tester (such as the pin), applied load, testing medium (in air or aqueous solution), radius of the wear track, temperature, testing time and sliding distance can all be controlled.

Figure 1.7 shows different settings and relative motions between testers and samples. Different geometries have been designed for the wear in a specific mode. For example,

figure 1.7 (a) shows that a testing pin loaded on a surface to test the wear resistance, is fixed and applied a certain amount of stress. Localized deformation is created in the region where the disc is in contact with the pin. As the pin rotates with a controlled speed, the deformation region expands to a circular wear track from the wear of the pin. Useful data can be obtained during the entire sliding test, from the initial indentation of the pin to the generating sliding wear, then to the final stage of remove of the pin. The wear behavior can be analyzed from these data: the coefficient of friction, applied normal force, friction force, the sliding speed and distance, position and depth of the indenter.

The other sliding wear systems are very similar. A block is placed and applied a certain force at the rim of a disc to perform the wear test in figure 1.7 (b). The on-going frictional force is recorded during the rotation of the ring against the block. Wear rates of the block and the ring can both be obtained from the materials volume loss after the friction. This method can be used to measure a wide range of materials' frictional combinations. The time, lubrication, temperature and sliding velocity can all be adjusted.

A pin is applied to a linear reciprocating plate's surface in figure 1.7 (c). The plate moves against a stationary pin with a set frequency and a fixed sliding speed, which generates a linear wear track. The values of coefficient of friction generally change between positive and negative values due to the opposite direction of the relative motion.

Two discs can be used together to execute the wear investigation. They can be placed rim-to-rim as twin discs, as shown in figure 1.7 (d), which is commonly used to test railway

materials. The twin disc geometry produces the tangential force and creepage, which can

simulate surfaces in rolling-sliding contact (wheel/rail). This technique can be used to study

the rolling contact fatigue, wear and other issues related to wheel/rail contact. Two rings

can also be placed with flat surfaces against each other, as illustrated in figure 1.7 (e). In

this case, worn regions between two rings always keep in contact throughout the running

of this system.
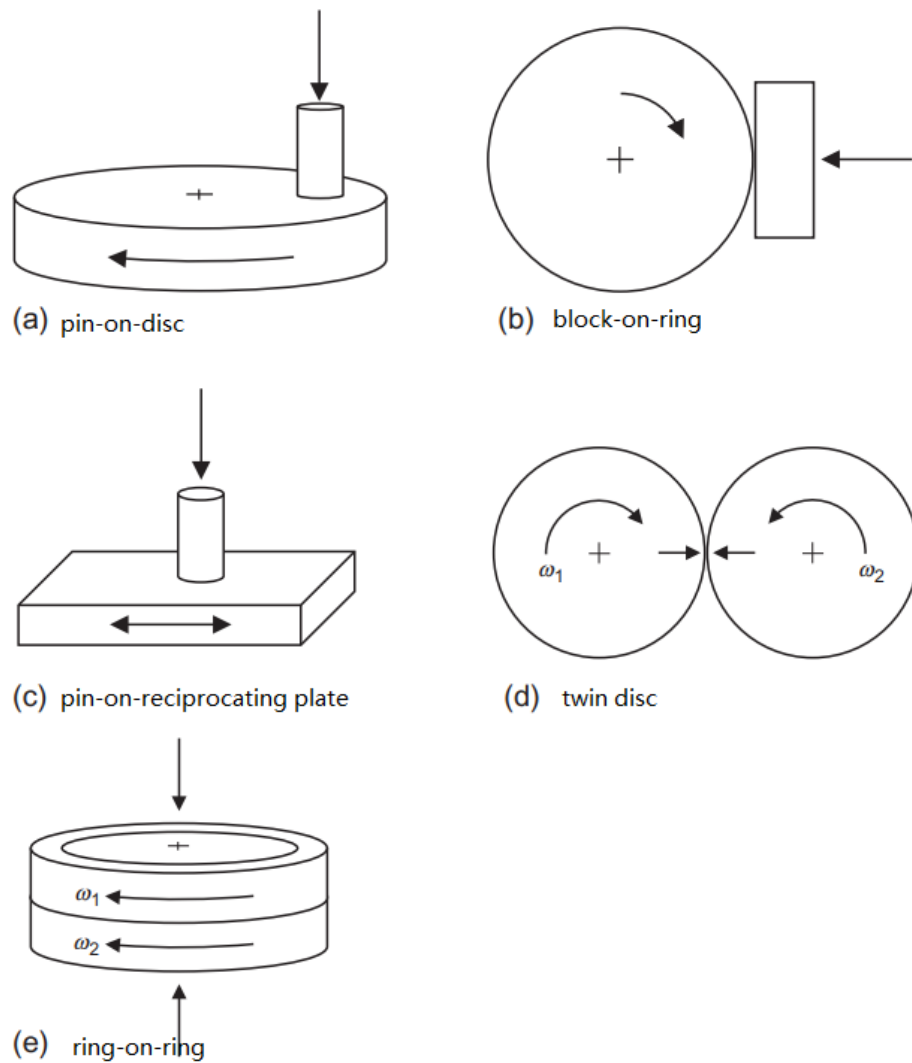
Figure 1. 7 Sliding wear test systems with different geometries [30]

1.2.3 Anti-wear techniques

Selection of Materials and surface modification

Improving and selecting materials with good wear resistances is a simple way to reduce the wear damage to equipment, such as wear resisting steel, carbide alloy and ceramic materials.

Surface chemical and heat treatments are common ways to enhance the surface wear resistance. The carburizing, nitriding, boriding, chromizing treatment can be applied to increase the hardness, resistance to wear. Figure 1.8 [31] shows these surface diffusion processes to the hardness of steel. According to the Archard's wear equation, the increase of the hardness generally implies the improvement of the wear resistance. On the other side, instead of enhancing the surface hardness, sulfurizing and oxidizing processes can modify the surface tribology property and form a solid lubrication film over bulk materials [32]. By introducing this lubrication layer, the adhesive effect and the fatigue wear can be reduced.
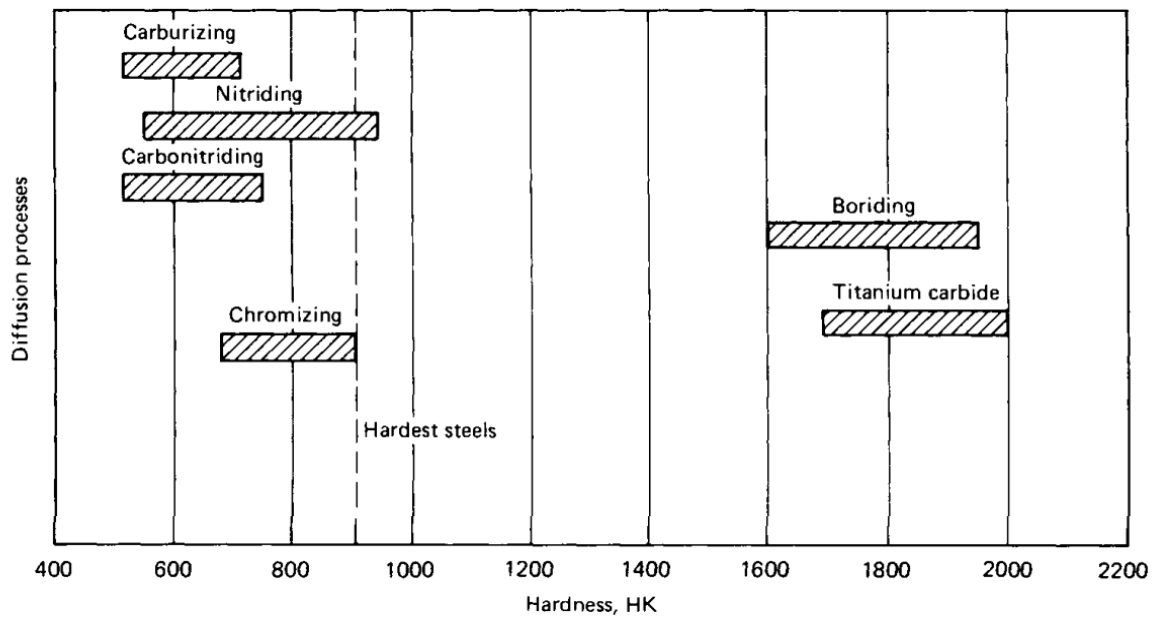
Figure 1. 8 Hardness for different element diffusion of steel [31]

Besides, shot peening [33] can also be used to strengthen the materials' surfaces and increase the fatigue life by introducing the surface plastic deformation and the cold work hardening. Shots made from metal or ceramic are controlled and directed to impact the surface with a high velocity. There are two major types of changes within the deformation layer. First, the grain refinement occurs. The dislocation density and the disorder of lattices are greatly increased. Second, a high residual compressive stress is introduced within the deformation layer. Both mechanisms exist and contribute to the hardening for most materials. However, the first mechanism of grain refinement is more characteristic in softer materials, while the second mechanism of residual compressive stress is more dominant in harder materials. B.K.C. Ganesh [34] et al demonstrated the positive effect of shot peening on the wear resistance and tensile strength of titanium alloys. It was shown that the wear

20

rate of Ti–6Al–4V alloy was decreased by 51.6% and 55.0% after the peening treatment at 3.5 bar and 4.5 bar, respectively. The microhardness was also increased due to the treatment. The same positive effect of the treatment on wear resistance and hardness also exhibited on Ti–6Al–7Nb alloy. The ultimate tensile strength of Ti–6Al–4V alloy was also improved by 150 MPa. The induced strain hardening and compressive residual stress contributes to the overall enhanced surface strength.

Table 1. 1   Properties of titanium alloys after shot peening treatment [34]

Alloy	Condition	Surface roughness of wear track (Ra) (μm)	Microhardness $HV_{(0.5)}$	Wear rate ($\times 10^{-11}$ m^3/m)
Ti–6Al–4V	No peening	0.016 ± 0.002	326 ± 1	2.016 ± 0.110
	Peening 3.5 bar	1.67 ± 0.06	412 ± 47	0.976 ± 0.012
	Peening 4.5 bar	2.27 ± 0.12	439 ± 66	0.907 ± 0.079
Ti–6Al–7Nb	No peening	0.609 ± 0.008	319 ± 1	0.974 ± 0.132
	Peening 3.5 bar	1.73 ± 0.10	377 ± 20	0.807 ± 0.012

Alloy	Condition	Surface roughness of wear track (Ra) (µm)	Microhardness $HV_{(0.5)}$	Wear rate ($\times 10^{-11}$ m^3/m)
	Peening 4.5 bar	1.96 ± 0.03	352 ± 16	0.786 ± 0.004

In addition to enhancing the strength of bulk materials, coatings with better wear resistances, can be applied through electroplating [35], physical and chemical vapor deposition [36].

Lubrication [37] has a large effect on materials wear performance. Lubricants can be added in between two frictional surfaces to reduce the coefficient of friction and improve the machine work efficiency. Besides, the lubrication reduces the wear damage, prevent the overheating and dust, and extending the machine lifetime. Common lubricants include lubricating oil, grease and solid lubricant such as graphene, MoS2. Lubricating oil with a large viscosity is generally used for the work condition of low motion speed, high load and high temperature. Meanwhile, lubricating oil with a small viscosity is usually used for the system with the high motion speed, low load and low temperatu1re. Lubricating grease is generally used in low working speed and the environment with dust.

1.3 Cu and its alloy

Corrosion of metallic materials in marine environment is a main issue for the safety of maritime transportation and offshore oil drilling operation, which leads to a huge cost for

facility maintenance and replacement [38]. Different materials and anti-corrosion techniques are developed to improve the durability of relevant machinery and facilities with reduced costs. Due to its corrosion resistance and modifiable mechanical properties, Cu alloy has found a wide variety of applications especially in the marine environment [39-42]. The corrosion resistance of Cu in water is due to the formation of a protective oxide film, Cu_2O, on the metal surface [43]. The chloride ions in seawater can increase the corrosion rate. Generally, the corrosion rate is very high at the beginning when a copper product first contacts the water. However, the corrosion rate decreases as the Cu_2O film forms and thickens. The rate turns to be very slow after a stable oxide film is formed. During this process, the dissolution of the oxide film into the water at the film-water interface slowly continues, while ions from metal surface continue to form the new oxide layer. The aqueous environment can be saturated due to the dissolution of the oxide film without too much turbulence of the water. Thus, an outer film can be deposited on the oxide film. This outer film does not exbibit a good protective effect on corrosion and its chemical composition depends on the aqueous environment. For example, an outer film of $Cu_2Cl[OH]_3 \cdot 4H_2O$ is formed in a high chloride environment, while an outer film of copper sulfate is formed in soft waters.

Cu alloys are electrically conductive and their non-sparking and non-magnetic properties make them also suitable for working in environments such as oil refineries, chemical plants and underground mining [44]. The early pipeline system in the seawater

environment was made of carbon steel and cast irons with relatively low cost. However, their low resistance to corrosion and fouling make the ferrous alloys performed poorly with a short service life. Copper became the base metal for a wide range of applications in the marine environment, which can be strengthened by alloying elements. Nickle is one of the common alloying elements used to increase the mechanical strength and corrosion resistance of copper. The nickel addition increases the strength of copper with raised corrosion resistance in seawater, superior biofouling resistance and good ductility [45].

North and Pryor showed that the corrosion resistance of Cu alloy is improved in 3.4% NaCl solution with an increased content of Ni [46]. As illustrated in figure 1.9, the weight loss of Cu was greatly decreased with a 10 wt.% Ni addition. 70Cu-30Ni sample also showed a similar trend of improving the corrosive weight loss. It was demonstrated that the corrosion resistance of the Cu_2O oxide film is strengthened due to the addition of nickel. There exist a large number of cation vacancies inside the Cu_2O oxide film which is formed on pure copper in water. Thus the diffusion of copper ions through this film is relatively easy. Besides, the electronic resistance is very low due to the high concentration and mobility of the positive hole inside the film. With the addition of nickel to copper, nickel is incorporated into the vacant lattice sites of the oxide film and results in a decrease of positive holes. It was shown that the electron and ion resistances of the Cu_2O film are increased with the Ni addition, which contribute to an improved overall corrosion resistance of CuNi alloys.

24
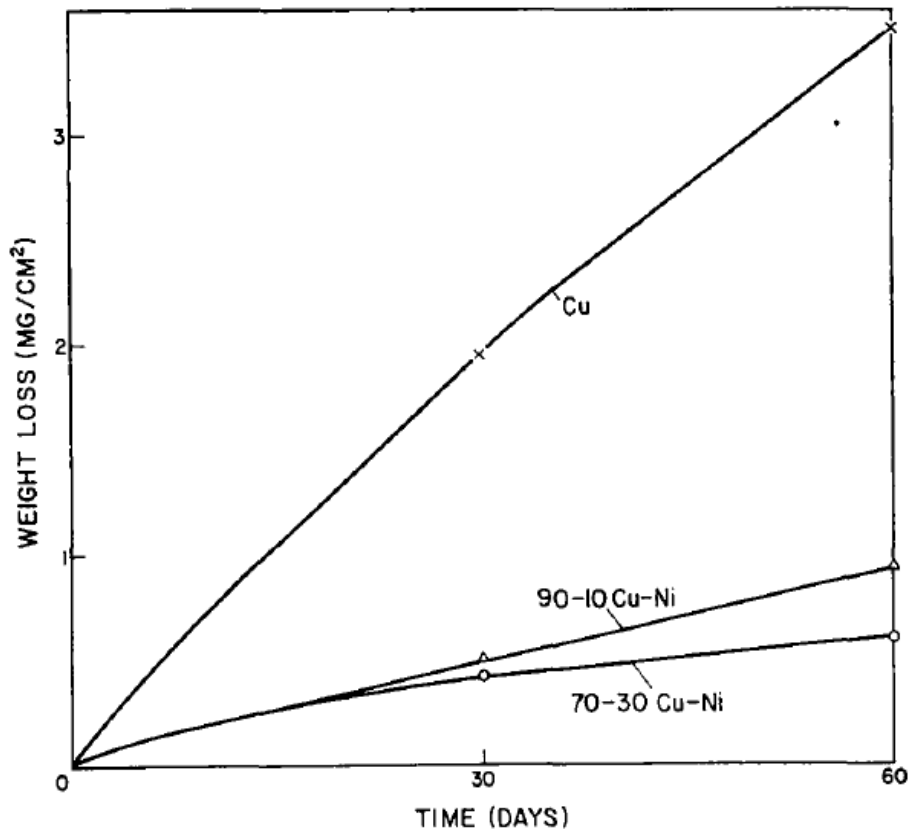
Figure 1. 9 Weight loss of Cu, 90Cu-10Ni, 70Cu-30Ni in boiling 3.4% NaCl solution [46]

However, though Cu alloys have high corrosion resistance, their mechanical strength is still not as high as wished.

Copper can be strengthened by other alloying elements as well [47-49], e.g., Zn, Tin, Al, Si, and Fe. Brass is a commonly used material consisting of copper and zinc. Zinc helps increasing the strength of Cu by forming a 2nd phase after the zinc composition exceeds 32.5 wt.%. The hardness of the CuZn alloy increases but its ductility decreases with increasing the zinc content. Lead is sometimes added to the alloy to improve its machinability.

Tin is also used as an alloying element to strengthen copper. Bronze is an alloy consisting of copper, tin and other additives such as zinc, manganese and aluminum and silicon. Tin can enhance the corrosion resistance of copper and its strength as well. The small addition of tin may lead to a decrease in toughness, but the ductility could be recovered by heat treatment.

Aluminum brass shows its proof stress at 150 MPa and phosphor bronze has its proof stress at 120 MPa, while 70/30 copper-nickel shows its proof stress at 170 MPa. Beryllium copper has the greatest strength than any other Cu alloy with its hardness approaching to that of steel [50]. However, beryllium is a hazard material, generating safety issues during manufacturing of Cu-Be alloys. This prevents it from a wide range of applications.

More information on commonly used alloying elements for making Cu alloys and corresponding properties can be found in the literature [43]. In general, the mechanical strength of Cu alloys is still not comparable to that of steel, limiting their applications. It is thus highly desired that if the mechanical properties of Cu alloys can be brought closer to the level of steels while keeping their anti-corrosion capability.

In addition to the mechanical properties, the resistance of Cu alloys to wear and corrosive wear [51-53] is another important factor influencing their range of applications. Wear does not only cause the damage to the components, it may also lead to failure of the entire machinery system and generate safety issues. The situation may become more severe when wear occurs in a corrosive environment such as the marine environment.

Simultaneous corrosion can accelerate wear due to the synergy of wear and corrosion [54]. Thus, the materials used in the marine environment need to possess intrinsic corrosion resistance, which should come from high nobility of the material rather than from passive film since the passive film can be damaged when wear is involved.

1.4 Objectives of this study

In this study, effects of B and Mo on hardness and resistances of CuNi alloys to wear, corrosion and corrosive wear were investigated. The selection of B and Mo as the strengthening elements is ascribed to the facts that B can form hard borides in steel and some non-ferrous alloys [55] and Mo is one of common strengthening element for ferrous alloys [56]. Boron has been used to enhance the hardenability of steels [57]. The existence of boron atoms at grain boundaries decreases the energy and retards the generation of crystallization centers. Boron-added steels show higher mechanical strength and resistance to abrasion. The addition of Mo in steel improves not only the hardenability but also the corrosion resistance and weldability. Mo atoms act as the solute for solid-solution hardening can enhance the strength of materials at elevated temperatures. Mo has also been used to improve strength and corrosion resistance nickel-based alloy in solid-solution state [58]. HASTELLOY B-2 is a nickel-based alloy with 28wt.% Mo, which was developed to be used in acidic environments, particularly in hydrochloric acidic environments.

Objectives of this study are:

1) To investigate and evaluate the effectiveness of two elements, B and Mo, in

   strengthening CuNi alloys and their effects on the resistance of the CuNi alloys

   to wear, corrosive wear and corrosion;

2) To determine how much they could strengthen the CuNi alloy and understand the

   underlying mechanism.

Chapter 2 Experiment Procedure

2.1 Sample Preparation

Pure metal powders of Cu (99.9%, Strem Chemicals), Ni (99.9%, Strem Chemicals), Mo (99.95%, Alfa Aesar) and B (99%, Aldrich) were used to make designed alloy samples. The base Cu-Ni alloys were 50at.% Cu-50at.%Ni and 68 at.%Cu-32at.%Ni. Detailed compositions of B and Mo added samples are given in Table 2.1. Different materials were first weighted and then mixed together in a mould with a good resistance to high temperature. Then the materials and the mould were put into an arc melting furnace, as exhibited in figure 2.1. The furnace was then vacuumed and filled with argon gas. This process was repeated three times to minimize the existence of air. Then bulk materials of Cu-Ni and its modified alloys were fabricated with a melting arc generated from a tungsten electrode in an Ar environment. The samples were re-melted in the furnace three times to increase their microstructural homogeneity, which were then annealed at 600℃ in an argon atmosphere for 4 hours. Surfaces of the samples were polished progressively with sandpapers of 60, 80, 400,600, 800 and 1200 grit and finally by 1-micron alumina polishing paste.

Table 2. 1 - Designed combinations of Cu-Ni alloy

Sample number	Cu content (at.%)	Ni content (at.%)	Mo content (at.%)	B content (at.%)
1	50	50	0	0
2	48	48	4	0
3	48	48	0	4
4	48	48	2	2
5	40	40	10	10
6	68	32	0	0
7	65	31	2	2

Figure 2.1 Arc furnace used to make samples for the present study

2.2 Microstructure analysis

The samples were characterized by the Scanning electron microscopy (Zeiss Sigma 300 VP-FESEM) to investigate the surface morphologies. Regions with different microstructures were analyzed using a Bruker energy dispersive X-ray spectroscopy (EDS) system, and different elements compositions were then calculated. Crystal structures were analyzed with X-ray Diffraction (Rigaku XRD Ultimate IV).

2.3 Hardness test

Rockwell hardness of the samples was measured using a ZHR Rockwell hardness tester (ZwickRoell) using a 1/16" ball with a load of 100 kg. Four different regions of each sample were selected and tested, based on which average values were obtained.

Figure 2.2 ZHR Rockwell hardness tester

2.4 Wear and corrosive wear tests

Wear and corrosive wear behaviors of the samples were evaluated using a pin-on-disk wear tester (CSEM Instruments, Neuchatel, Switzerland). A silicon nitride ball with the diameter of 3 mm was used as a pin to create circular wear tracks on samples under a load of 10 N. The track diameter was set 2 mm and sliding speed was 1 cm/s. The test was performed in air (500 laps) and 3 wt.% NaCl solution (1500 laps), respectively. The test in NaCl solution was designed to investigate the materials performance under the environment of sear water. The sliding distance was designed three times longer in NaCl solution than that in air. It was due to the fact that it took more time to reach a stable wear stage in the NaCl solution with a stable coefficient of friction curve. The load, sliding speed and distance, temperature, abrasion pin were all controlled the same to for each environment

Wear tracks were then analyzed using a 3D Optical Surface Profiler (ZeGage, ZygoCorp), based on which the depth and areas of integrated wear track were determined and corresponding total volume loss was automatically calculated by ZeGage's software. The worn surface and the morphologies were also observed. The hardness and wear resistance of an annealed carbon steel (ASTM A109) were also tested for comparison.
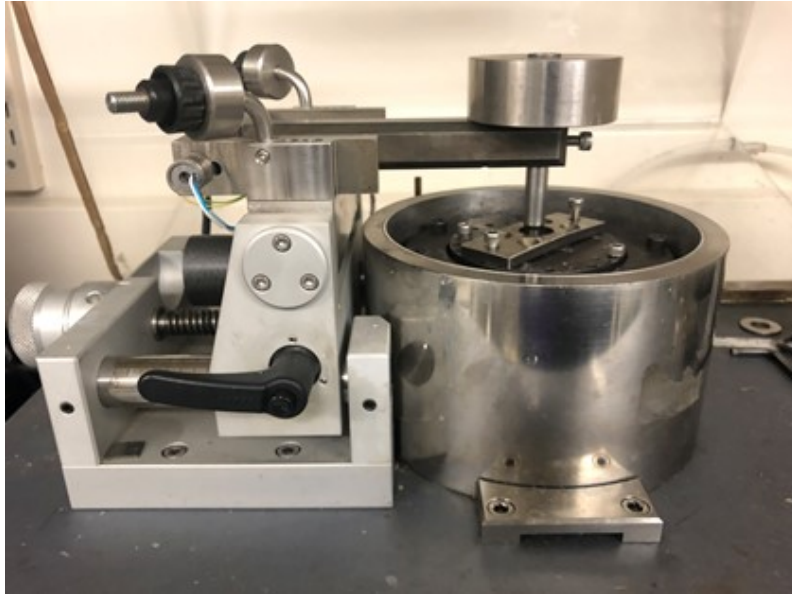
Figure 2.3 Pin-on-disk wear tester

Figure 2.4 3D Optical Surface Profiler (ZeGage, ZygoCorp)

2.5 Corrosion Test

The corrosion behavior of the samples was evaluated with polarization tests. Samples for the polarization test were sealed in epoxy resin. Only the polished surface of a sample was used for the electrochemical tests. Other parts of the sample were sealed in epoxy resin and isolated from the electrolyte solution. Liquid epoxy resin (West System, 105) and fast hardener (West System, 205) were mixed at a weight ratio of 5:1. Samples were then placed at the bottom of a mould. The upper sides of the alloy were connected with a copper conductor wire by copper adhesive tape. Liquid epoxy resin and hardener were then transferred into the mould. The sample was taken out after the liquid solidification (24 hour) of the epoxy resin with only the bottom side exposed to the air. The surface of the sample was then polished to remove any residual epoxy resin.

The samples sealed in epoxy resin were used as working electrodes for the corrosion test, as illustrated in figure 2.5. The Cu-Ni alloy working electrode was immersed in 3 wt.% NaCl solution with a three-electrode system, including a saturated calomel reference electrode and a platinum counter electrode. Open circuit potential was measured during 1200 seconds after the sample was immersed in the solution. For the linear polarization test, the scan range of the voltage was from -20 mV to 20m V with a scan rate of 0.1mV/s. Polarization resistance was then calculated based on the slope of the curve. The polarization test was done with a larger scan range from -0.4 V to 0.8 V and a scan rate of 0.5mV/s.
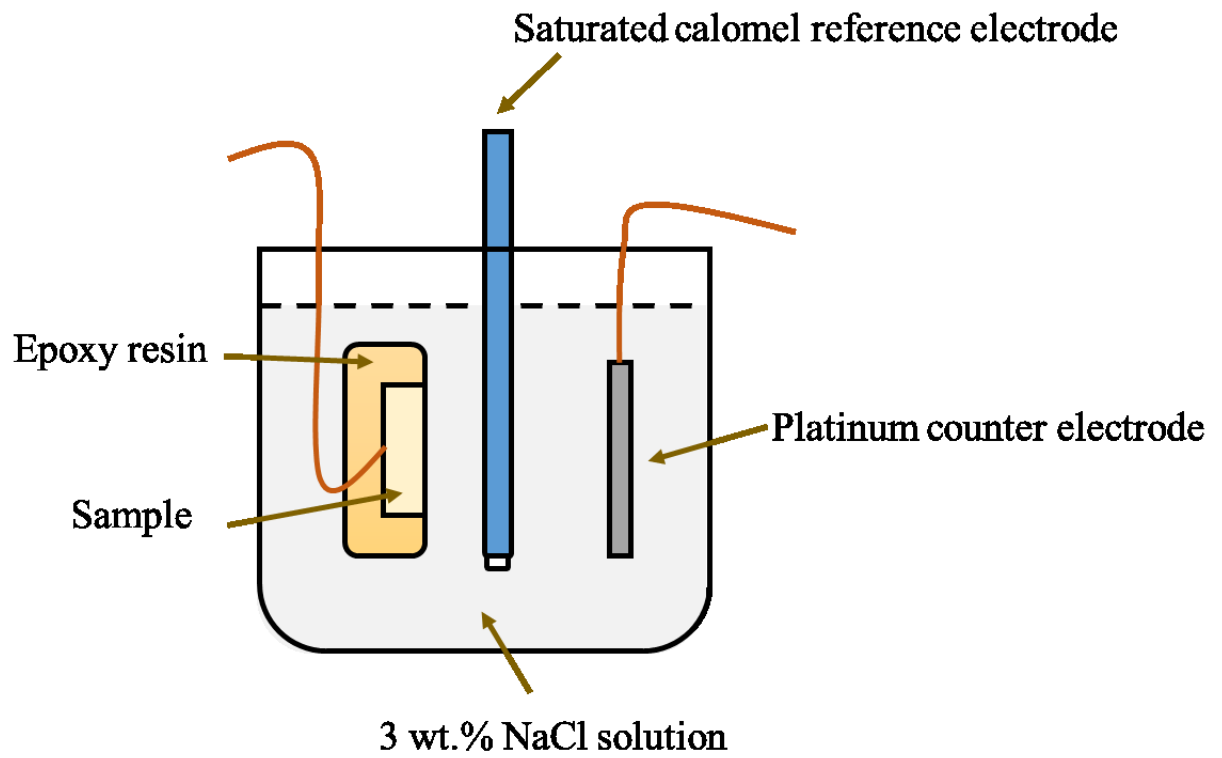
Figure 2.5 Schematic of the corrosion test: polarization and open circuit potential tests

Chapter 3 Materials Characterization

Microstructures of the alloys under study

SEM images and EDS analysis of the fabricated samples are shown in Figure. 3.1 and Table 3.1. Based on the SEM microstructure images, since Cu-Ni binary alloy is an isomorphous one, no second phases were observed in the 50Cu-50Ni alloy and 68Cu-32Ni. Second phases were observed after B and Mo were added. Different major phases are showed as lighter and darker regions in 2%Mo-2%B, 4%B, 4%Mo alloyed samples. Patches containing B and Mo were observed, which are particularly visible in the sample containing 10%Mo and 10% B additions as shown in figure 3.1 (e). Table 3.1 shows the overall element composition of different samples. It illustrates that the actual element compositions of samples are very close to the designed atomic percentage of Cu, Ni and the additive elements.
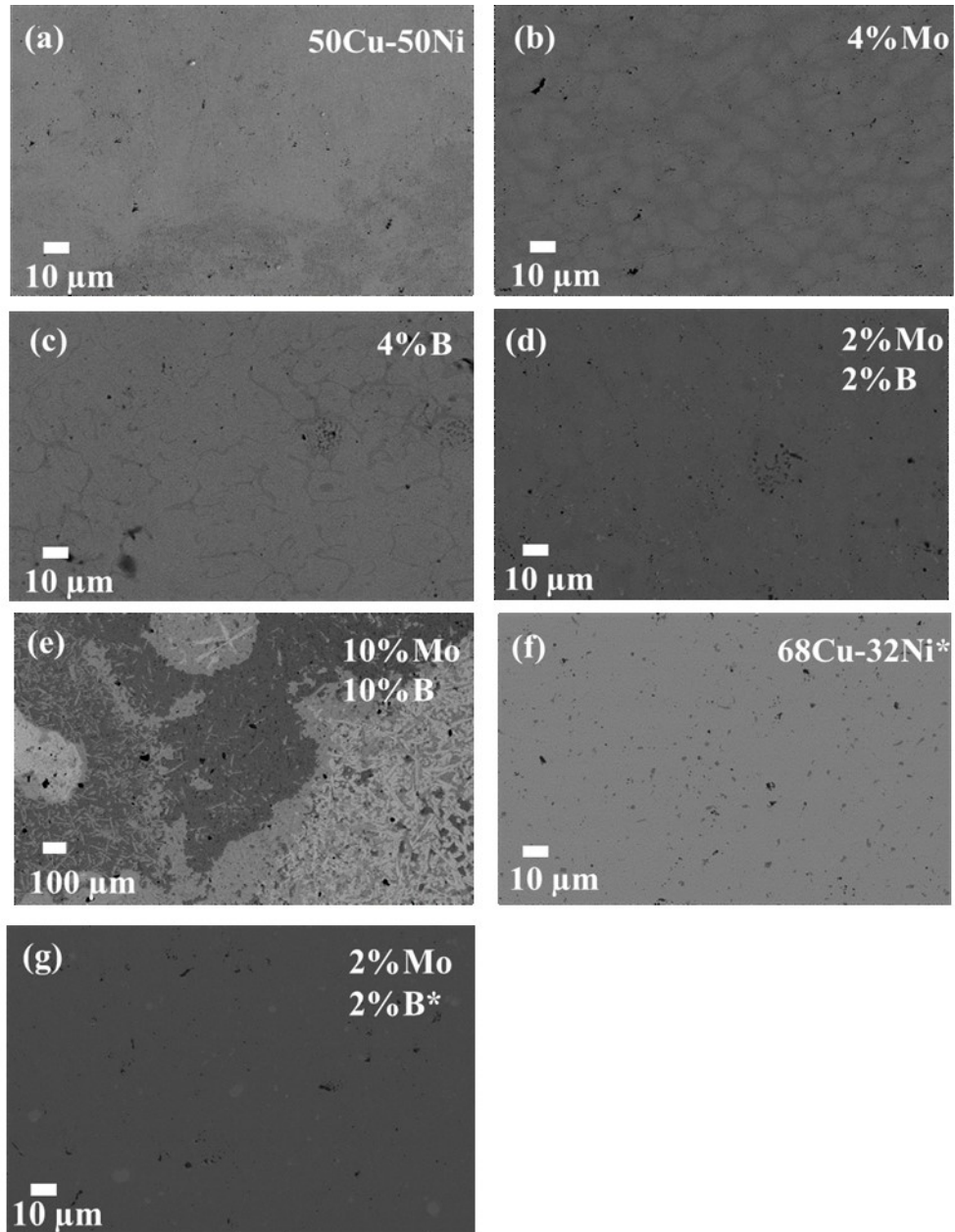
Figure 3.1 SEM images of (a) base alloy of 50Cu-50Ni and its modified alloys with added (b) 4%Mo, (c) 4% B, (d) 2%Mo-2%B, and (e) 10%Mo-10%B; (f) base alloy of 68Cu-32Ni and its modified alloy with added (g) 2%Mo-2%B.

Table 3. 1 EDS analyzation results

Sample	Cu content (at.%)	Ni content (at.%)	Mo content (at.%)
50Cu-50Ni	45.60	54.40	0.00
4%Mo	48.80	47.50	3.70
4%B	49.30	50.70	0.00
2%Mo-2%B	47.72	50.04	2.24
68Cu-32Ni*	69.60	30.40	0.00
2%Mo-2%B*	69.50	29.23	1.27

According to the XRD analysis figure 3.2 (a) and (c), both 50Cu-50Ni and 68Cu-32Ni alloys only show the phase of CuNi. For the 50Cu-50Ni with 10%Mo and 10%B additives, shown in figure 3.2 (b), phases like Ni_3B and Mo_2NiB_5 exist. Ni_3B and MoNi phases exist in 68Cu-32Ni alloy with 2%Mo-2%B, as indicated in (d). Cu-Ni alloy can be strengthened by introducing second phases. For example, Ni and B can react to form Ni_3B phase [59], which is hard and should increase the mechanical strength and wear resistance of Cu-Ni alloy. Molybdenum mainly exists as the form of MoNi and Mo_2NiB_5. The strengthening effect of the additive elements will be further discussed in the next chapter. Observed phases of these samples is summarized in table 3.2.
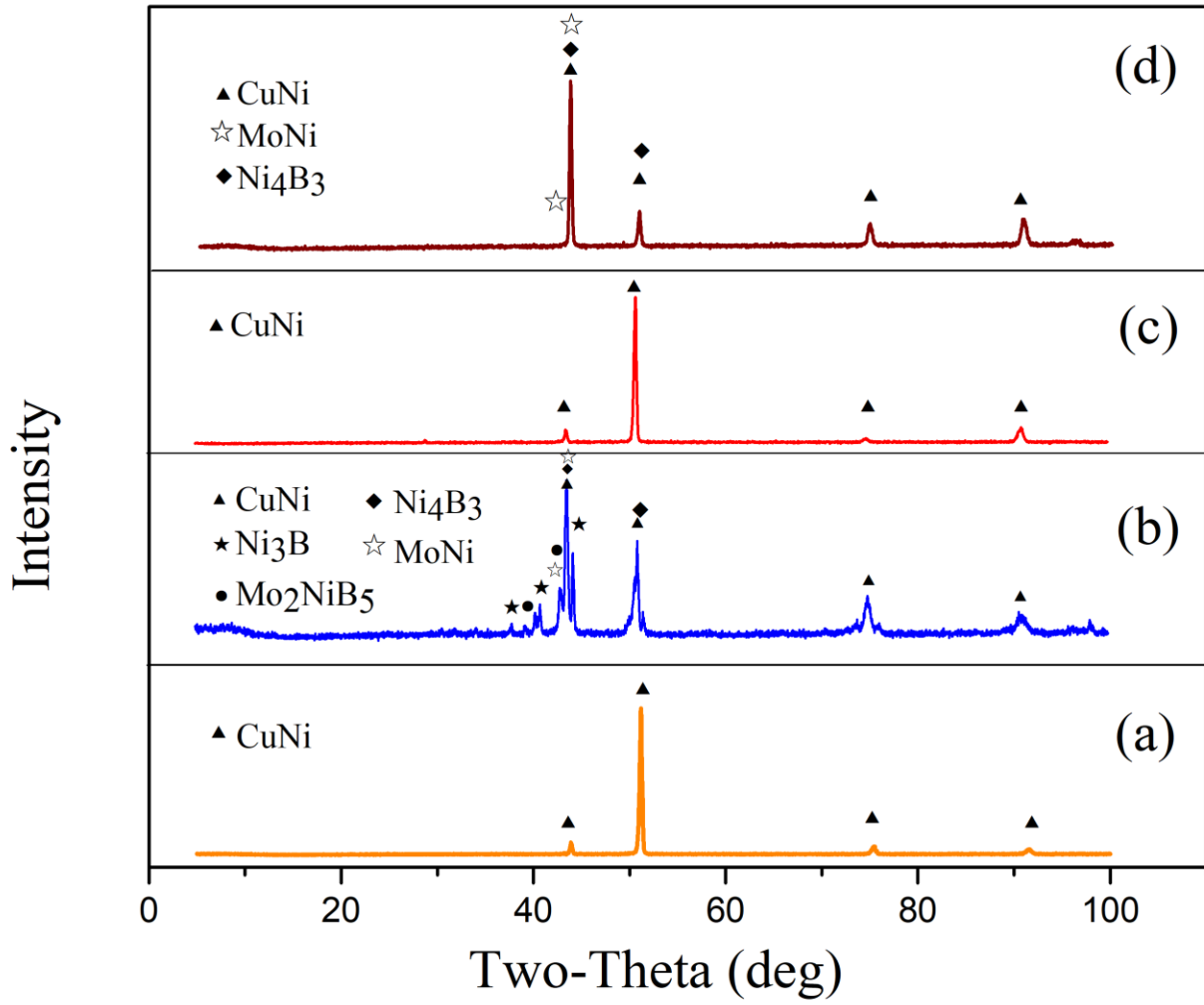
Figure 3. 2 XRD patterns of (a) 50Cu-50Ni and (b) its modified alloy containing 10%Mo-10%B; (c) 68Cu-32Ni and (d) its modified alloy containing 2%Mo-2%B*

Table 3. 2 Phases detected in each alloy

Sample	Detected phases
50Cu-50Ni	CuNi
10%Mo-10%B	CuNi, Ni_3B, $Ni_4B_3Mo_2NiB_5$, MoNi
68Cu-32Ni*	CuNi
2%Mo-2%B*	CuNi, MoNi, Ni_4B_3

Local compositional analysis was carried out using Energy-dispersive X-ray spectroscopy (EDS). Results of the EDS analysis are presented in Table 3.3 and corresponding spots for the compositional analysis are illustrated in Figure 3.3. However, the EDS examination is unable to detect boron due to its low fluorescence yield and absorption [60]. The peaks of light elements like boron are weak and covered by noise signals and those of heavier elements, making them indistinguishable. Besides, very few X-Ray signals are produced by boron with low energies, which are absorbed by the sample itself and the entrance window of detector. Thus, the amount of boron is not given in Table 3.1. However, it is illustrated that, for the rest of the elements, the actual element percentages are very close to designated values. The EDS result of 50Cu-50Ni sample with 10%Mo-10%B additives is not listed. Due to the existence of various second phases with very different element distributions, it is rather difficult to determine the overall element composition within a small area under analysis.
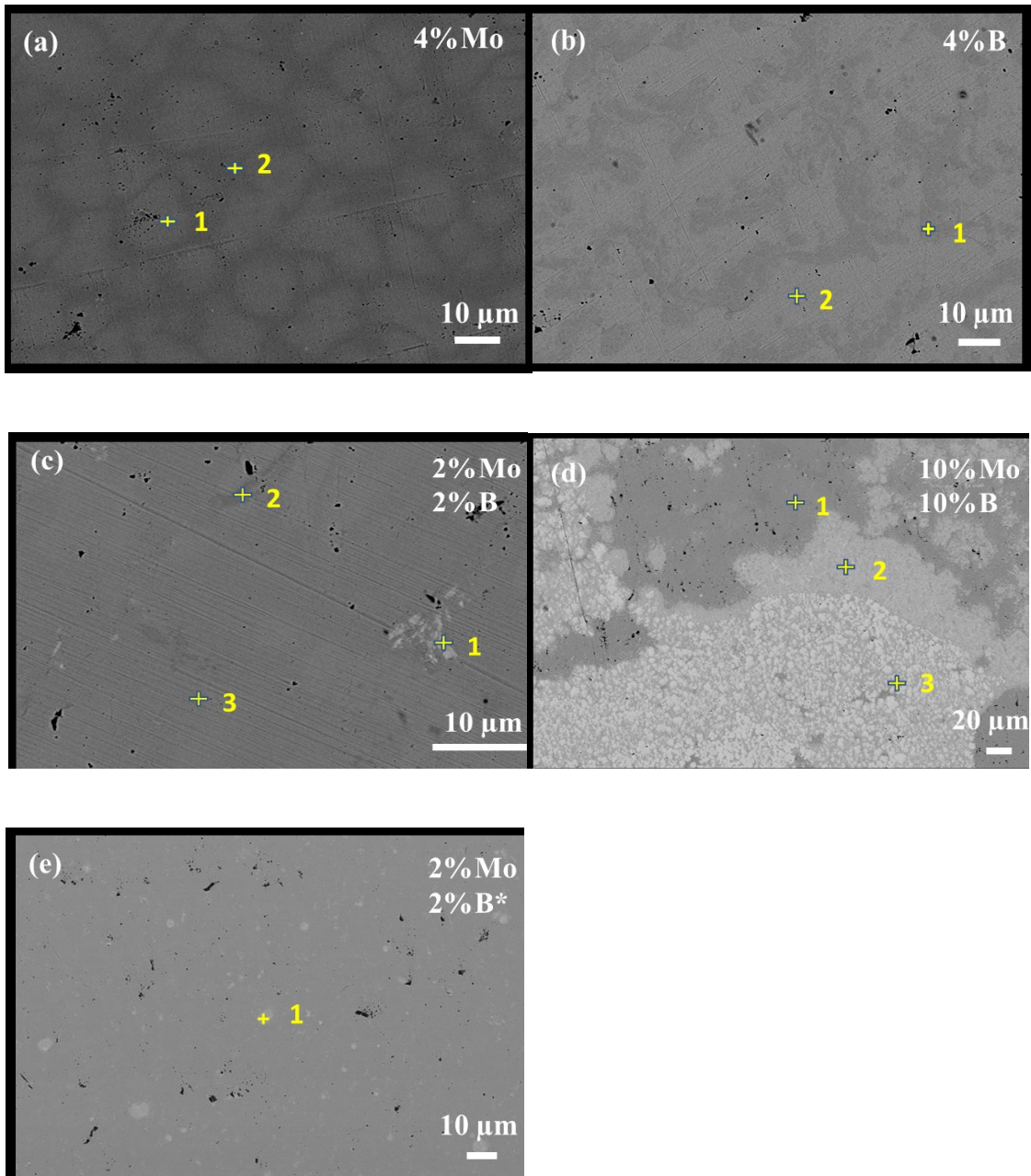
Figure 3.3 SEM images and EDS point analysis of (a) 4%Mo and (b) 4% B and (c)

2%Mo-2%B and (d) 10%Mo-10%B and (e) 2%Mo-2%B*

Table 3.3 EDS analyzation results of the selected points from Figure 3.3

Sample	Cu content (at.%)	Ni content (at.%)	Mo content (at.%)	O content (at.%)
a-1	32.23	61.28	6.49	0.00
a-2	55.62	43.05	1.33	0.00
b-1	14.19	84.07	0.00	1.75
b-2	50.94	49.06	0.00	0.00
c-1	13.04	49.52	34.97	2.47
c-2	12.81	86.38	0.81	0.00
c-3	38.30	57.90	3.30	0.50
d-1	52.92	43.42	3.66	0.00
d-2	2.60	40.74	56.66	0.00
d-3	0.96	1.37	88.20	9.47
e-1	29.96	47.02	23.02	0.00

Based on the SEM, EDS and XRD analysis, different phases were identified for samples with the addition of B and Mo. XRD analysis demonstrated the existence of second phases for B and Mo modified samples. For 50Cu-50Ni with 4%Mo addition, two major phases were observed from SEM images and regions with different morphologies were analyzed by EDS. To obtain SEM images, the electron beam interacts with the sample and

backscattered electrons are reflected. The point EDS analysis of Figure 3.2 (b) showed very different Cu and Ni element distribution due to the existence of boron, which was undetectable by EDS. It was clearly demonstrated by the SEM image that the different phases show different colors and morphologies. For the 50Cu-50Ni with 2%Mo-2%B addition, the composition of Mo varied from 0.81% to 34.97% within different phases based on table 3.3. Similarly, the 10%Mo-10%B modified sample showed various phases with very diverse elements composition. The darker region, such as d-1 in figure 3.3 (d), mainly contained Cu and Ni with less Mo concentration. For region such as d-2 and d-2, it was illustrated there was very few Cu concentration. Instead, Mo content became more dominant in these regions.

In the isomorphous CuNi alloy, a small addition of Mo and B would have many possible phases. Due to the lack of ternary phase diagrams of Cu-Ni-Mo and Cu-Ni-B, possible phases are discussed based on the binary phase diagrams. Assuming one additive element is completely mixed in either Cu or Ni matrix, a maximum value of the weight fraction of these additive elements in the matrix can be calculated, the results of which are listed in table 3.4. However, since only two elements are considered for each case in this assumption, these maximum values can be bigger in the real case due to the existence of other elements.

As indicated in table 3.2 certain phases were detected in each sample from XRD analysis. Cu-B and Cu-Mo phase diagram is illustrated in figure 3.4 (a) and (b). It is

illustrated that in Cu-Mo binary system, the solubility of Mo in Cu under 1000k is very

small. Thus, no intermetallic compound is formed with an up to 27.2% Mo and 5.9% Mo

in 50Cu-50Ni and 68Cu-32Ni, respectively. In the Cu-B eutectic system, the solubility of

B in Cu is only 0.01 wt.% at room temperature. Thus, no compound phase is generated

during the melting and cooling process. These results are consistent to the detected

phases from the XRD test, which does not show any Cu compound phase with B or Mo.

The maximum possible weight fractions of Mo in Ni are 28.9 wt.% and 6.3 wt.% in

two different samples. As illustrated in figure 3.4 (c), possible second phases based on the

phase diagram include $MoNi_x$ (x=1, 2, 3, 4, 8). The XRD result indicates the existing phase

of MoNi, which is not an exhibited at the room temperature. This can be due to the

relatively rapid cooling down rate and the short annealing time to the sample.

Table 3. 4 Estimated weight fraction of elements

Sample	Weight fraction of Mo in Cu (up to wt.%)	Weight fraction of B in Cu (up to wt.%)	Weight fraction of Mo in Ni (up to wt.%)	Weight fraction of B in Ni (up to wt.%)
50Cu-50Ni with 10%Mo-10%B	27.2	4.1	28.9	4.5
68Cu-32Ni with 2%Mo-2%B	5.9	0.7	6.3	0.7

(a)

(b)

(c)

45

(d)

Figure 3. 4 Phase diagrams of (a) Cu-Mo [61] (b) Cu-B [62] (c) Mo-Ni [62] (d) Ni-B [62]
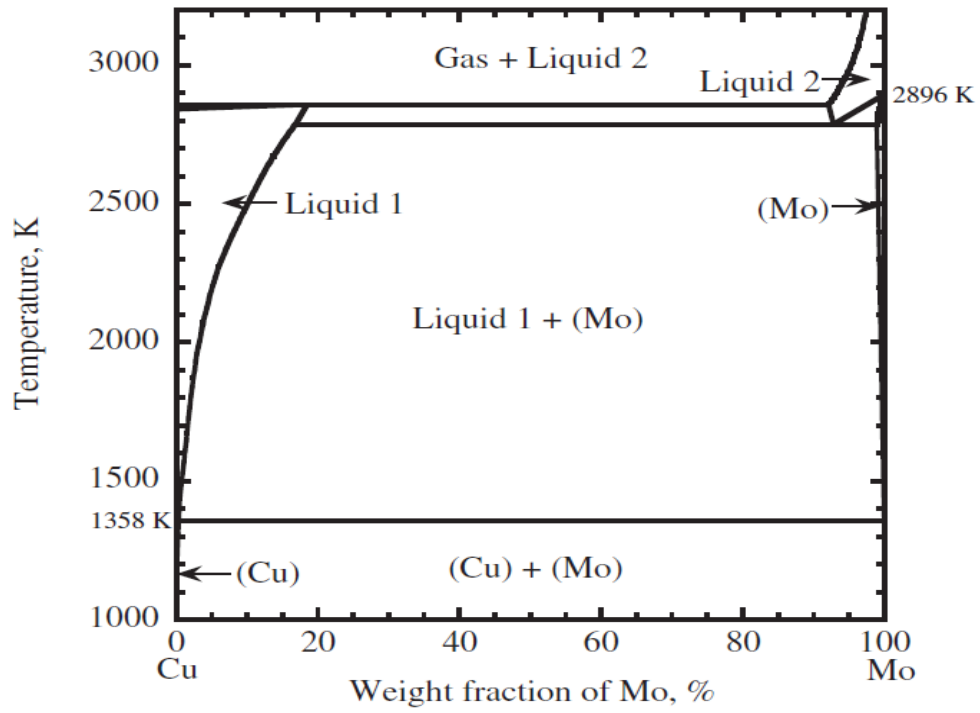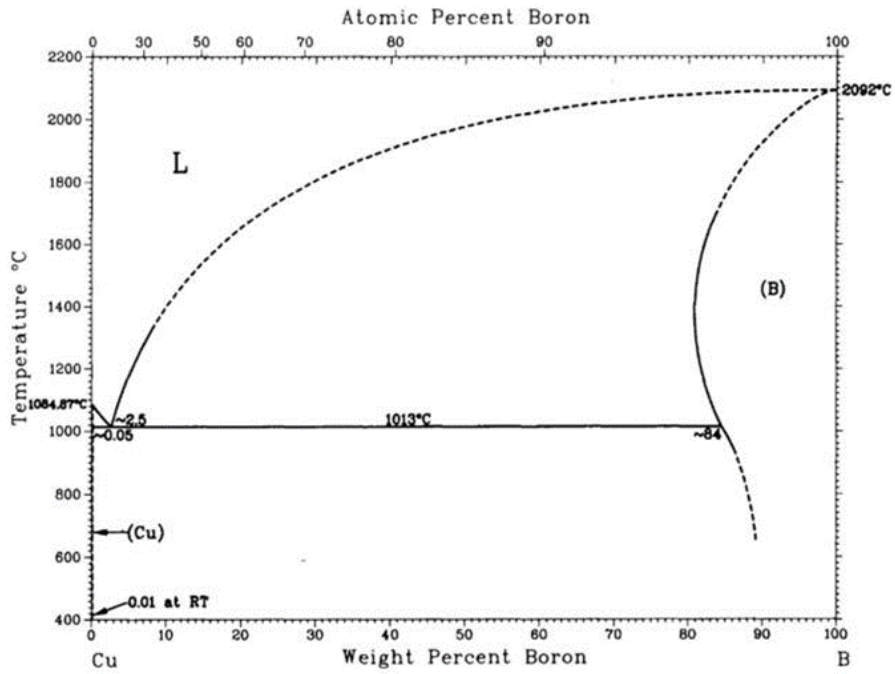
Figure 3.4 (d) shows the phase diagram of Ni-B. Different types of nickel borides can be formed. Ni_3B and Ni_4B_3 phases are detected in the sample. For the regions in the sample with the B content smaller that 6 wt.%, it is more likely to form the compound phase of Ni_3B. However, due to the existence of Mo and Cu, and an uneven distribution of B in Nickel, the formation of other nickel borides can also be possible, such as the Ni_4B_3 phase in 68Cu-32Ni with 2%Mo-2%B addition.

The Vickers hardness of Cu is 343-369 MPa [63] and the Vickers hardness of Ni is 638 MPa [63]. For the additives of Mo and B, their Vickers hardness values are 1400-2740 MPa [63] and 4900-5800 MPa [64], respectively. Finch CB et al. showed the mechanical properties of Ni_3B, which has a Vickers hardness of 10490 MPa to 10750 MPa [59] based on different lattice orientations. The Vickers hardness of Ni_4B_3 reported by Motojima S [65] is 15690 MPa. MoNi phase has a Vickers hardness of 8924 MPa [66]. These hardness values are summarized in Table 3.5 for comparison.

It is shown that Cu has the lowest hardness among the possible phases in table 3.5. The generation of the phases detected from XRD, all have relatively high hardness. For example, the phase of Ni_3B has a hardness nearly 28 times larger than that of Cu. The hardness of these phases could be an indicator to understand the mechanical properties of modified Cu-Ni alloys.

Table 3.5 Information on hardness of relevant phases

Phase	Vickers hardness (MPa)
Cu	343-369 [63]
Ni	638 [63]
Mo	1400-2740 [63]
B	4900-5800 [64]
Ni_3B	10490-10750 [59]
Ni_4B_3	15690 [65]
MoNi	8924 [66]

Chapter 4 Hardness and Resistance of the Alloys to Wear and Corrosion

4.1 Hardness test

It was demonstrated that the Mo and B additives were effective in strengthening the Cu-Ni alloy as shown in figure 4.1. Hardness of 50Cu-50Ni alloy was increased by 80% when 2% Mo-2% B were added, and by 110% when 10%Mo-10%B were added, respectively.
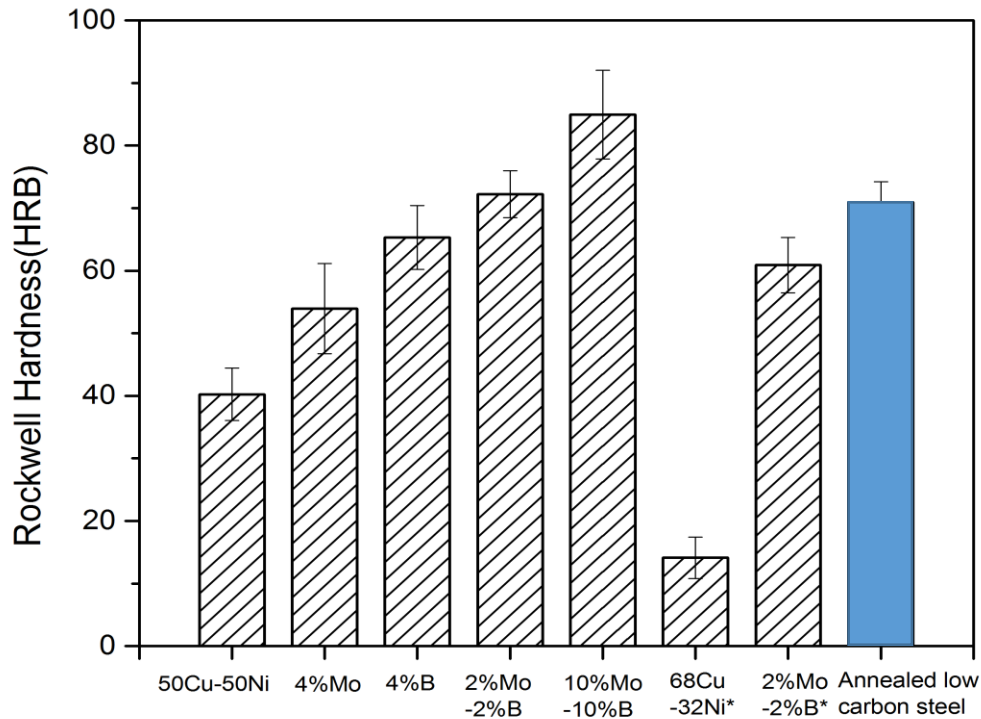
Figure 4. 1 Rockwell Hardness of samples with different additives

The combination of Mo and B additives was more effective than a single additive to harden the alloy. As shown, the addition of 2%B-2%Mo was more effective than 4%B or 4%Mo when added to Cu-Ni to increase its hardness. This should be attributed to the formation of more complex 2nd phases such as MoNi, Ni_3B, Ni_4B_3 and Mo_2NiB_5. B was more effective in hardening than the same atomic amount of Mo, which should be benefited from formed borides. As shown in table 3.5, the Vickers hardness of Ni_3B is 10490-10750 MPa while the hardness of MoNi is 8924 MPa. Thus, second phases with higher hardness, such as nickel borides, contribute to an overall higher hardness of the alloy.

As illustrated in figure 4.1, 68Cu-32Ni (which is 70Cu-30Ni in wt.%), a grade Cu-Ni alloy particularly popular in marine and offshore applications, has lower hardness than 50Cu-50Ni. This can be explained from the perspective of electron work function (EWF) [67]. Electron work function refers to the minimum energy to move an electron from inside a material to the vacuum outside the material. As demonstrated in figure 4.2 (a), the overall EWF is increased with an increasing content of Ni. This is due to the fact that the EWF of Ni, 5.04-5.35 eV, is higher than that of Cu, 4.53-5.10 eV [68]. The hardness of samples shows a similar trend as the EWF value, as shown in figure 4.2 (b). It is indicated that the addition of Ni to Cu contribute to the density of valence electrons in the alloy. This leads to stronger electrostatic and atomic interactions, which contributes to an elevated atomic bond strength. A high EWF value refers to a more stable electron state in metals. Young's modulus is also increased due to the stronger bonds. The stronger interaction between

atoms results in a higher energy barrier to the motion of dislocations. Thus, an overall improvement in hardness was observed with an increasing Ni content.

(a)
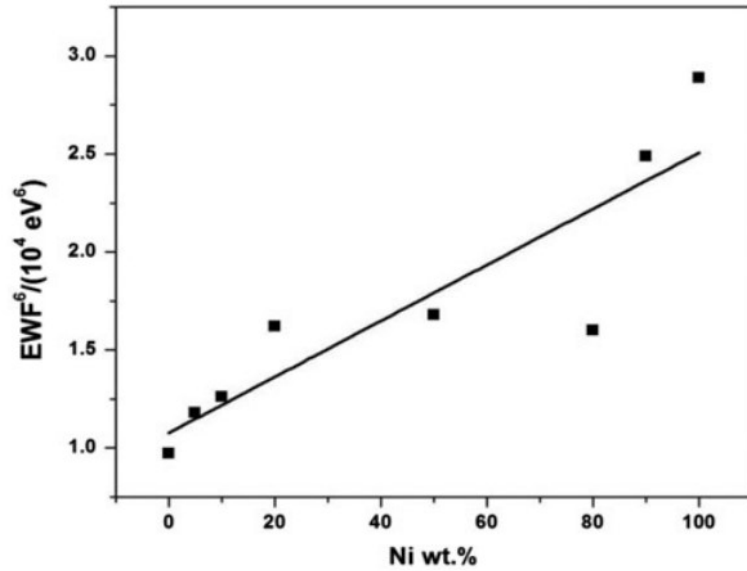
(b)
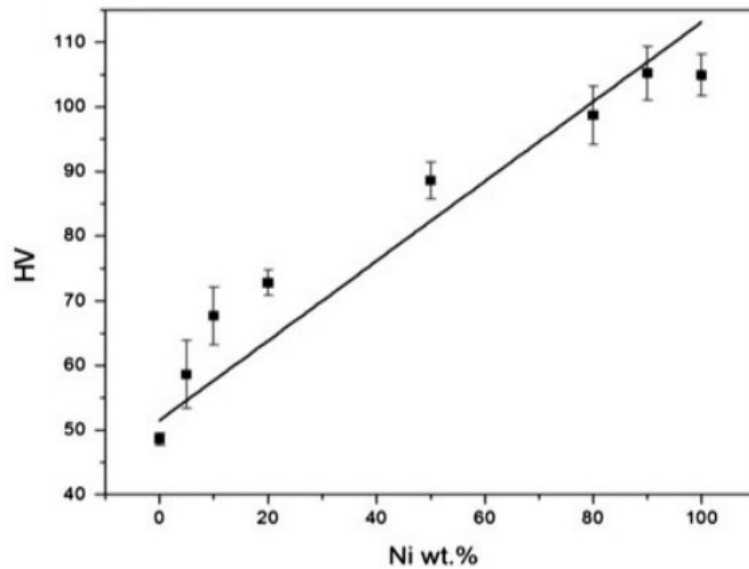
Figure 4. 2 (a) Electron work function (EWF) values and (b) Hardness of CuNi alloys with different Ni content [67]

With the addition of a combination of 2% Mo and 2% B, the hardness of 68Cu-32Ni was increased by 3 times. Hardness of annealed carbon steel (ASTM A109) was measured and presented in figure 4.1 for comparison. As demonstrated, the modified Cu-Ni alloy samples show their hardness comparable to or higher than that of the steel. Along with high corrosion resistance, the increase in hardness of Cu alloys in such a scale would significantly increase the competitiveness of Cu alloys for a wide range of industrial applications.

4.2 The dependence of the wear resistance on hardness

The frictional wear of the tests is closely related to the sliding condition, such as the applied load, sliding distance and velocity. As stated in the previous chapter, Archard's wear equation shows the relationship between the wear behavior and the factors influencing the abrasive wear.

The materials volume loss V caused by wear is related to the load between two surfaces W, the relative sliding distance X, hardness of the weaker surface H, and the dimensionless wear coefficient K. The volume loss can be calculated by

$$V = K \frac{W}{H} X \tag{4.1}$$

Based on the equation, the wear volume loss is proportional to the wear coefficient, applied load and the sliding distance, while inversely proportional to the hardness. To

compare the wear resistance, the applied load, sliding distance and velocity are all controlled as the same. Thus, the wear resistance can be estimated based on the hardness and coefficient of wear.

Preston et al.[69] developed the equation to reveal the factors to both adhesive and abrasive wear. In a specific wear test, the hardness of the upper layer can be uncertain and different from the bulk material. Thus, the ratio of K/H in equation (4.1) is replaced by a dimensional wear coefficient, Kw, with units of mm^3/Nm. Kw represents the wear volume per unit sliding distance under per unit normal stress. It is related to the intrinsic properties of materials and the operating settings of the wear test.

$$V = K_w WL \tag{4.2}$$

Spherical pins were used in this test to conduct the wear performance evaluation. J Kauzlarich et al. [70] showed some more detailed calculations of the wear based on the wear equation (4.2). It is illustrated that Archard's wear equation can be generally applied on a microscopic scale. However, for the pin-on-disc wear testing equipment, as shown in figure 4.3, the contact area and conditions change as the wear test runs. The tip of the spherical pin gradually wears away and generates a small flat worn out surface. The contact area between the pin and the sample surface grows. Thus the actual wear loss cannot be accurately described as a proportional relationship with the sliding distance.

J Kauzlarich et al set up a model of a special pin sliding over a flat surface. In this model, they showed the relationship between the applied load W, wear depth Δ, the radius

of the spherical pin r, and the wear volume loss V, and the dimensional wear constant Kw,

and N (the ratio of sliding distance to the slider radius, i.e. N= L/r)
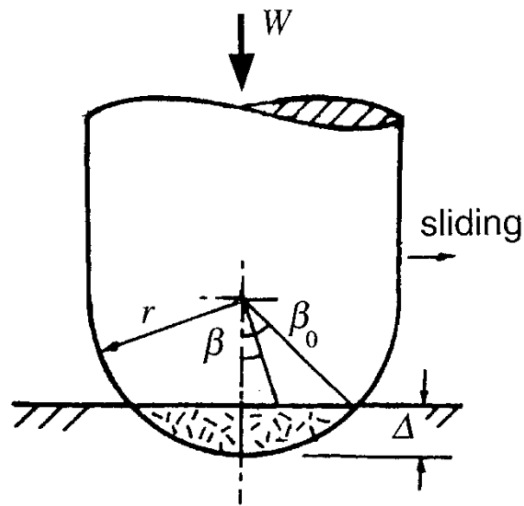
Figure 4. 3 Schematic of the pin-on-disc machine [70]

It is illustrated that when β0 is small, the wear volume loss still follows the relation of

$$V = K_w WL$$

and

$$\frac{\Delta}{r} \approx \sqrt{K_w PN} \quad (4.3)$$

Where the normal pressure P= W/(πr²)

However, when β0 is larger than π/2, this represents the situation that the tip of the

spherical pin has worn away and a prismatic contact has been generated. Then, it is shown

that:

$$\frac{\Delta}{r} \propto K_w PN \quad (4.4)$$

In our case, the sliding distance and the applied load are all controlled the same. For the wear condition of the slider, the tip was checked after every experiment and no prismatic contact was observed. Thus, the wear condition should be under the same law, and the wear resistances of the samples are closely related to the intrinsic materials properties, instead of other operation factors.

4.3 Wear and corrosive wear resistance

Resistances of the modified Cu-Ni alloys to wear and corrosive wear were evaluated using a pin-on-disc wear tester. Depth and width of the wear tracks can be measured using an optical profilometer.

The morphologies of sliding wear tracks are displayed in figure 4.4 and figure 4.5. The darker color represents a larger materials loss and thus a deeper wear track. In contrast, the lighter (yellow) color represents a smaller wear loss. For the wear test in 3 wt.% NaCl solution, it generally takes more time and distance to obtain stable wear coefficients than those in air. Thus, the sliding distance in NaCl solution is extended by 3 times larger than that in air. This leads to the wider wear tracks in 3 wt.% NaCl solution.
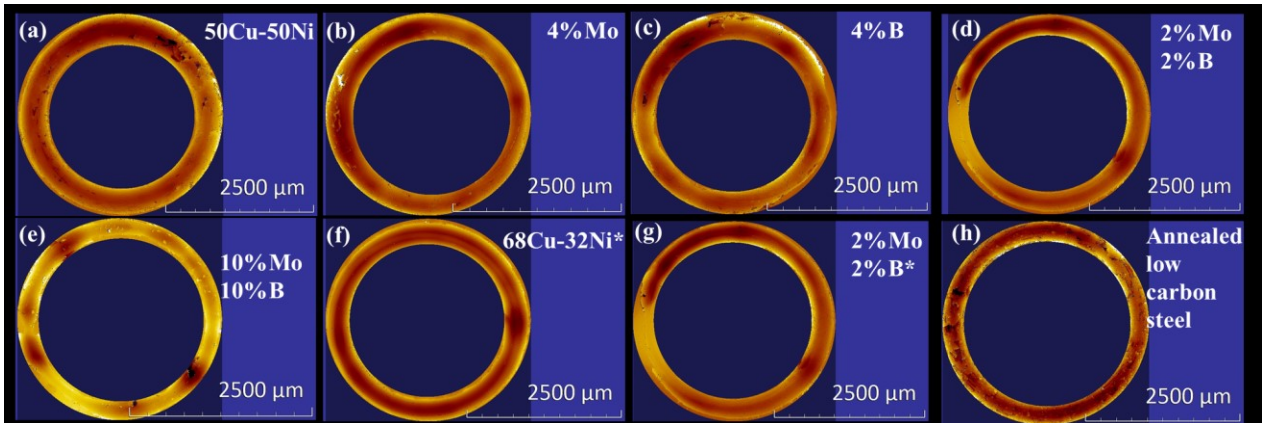
Figure 4. 4 Wear track profiles of sliding wear test in air
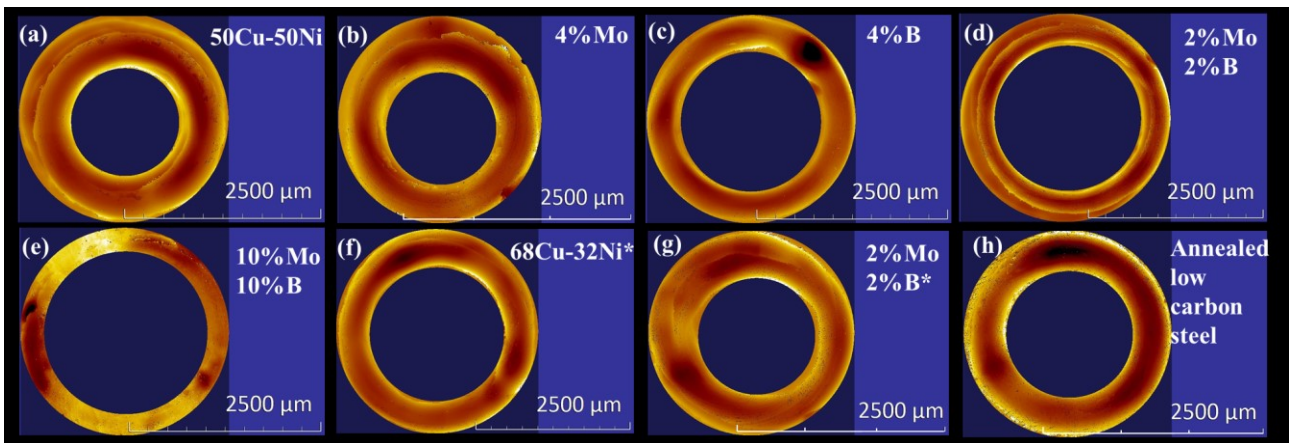
Figure 4. 5 Wear track profiles of sliding wear test in 3 wt.% NaCl solution

Profiles of wear tracks show different characteristics. The data is gained by selecting a cross-section of a wear track and measuring the depth and the width, illustrated in figure 4.6. The wear track cross-sectional distance refers to the width of the track and depth is compared to the flat surface of original materials. It is generally shown that, the depth and

the width of tracks decrease with the addition of Mo and B elements, for both sliding wear tests in air and NaCl solution. Thus, it leads to a smaller wear loss and a better wear resistance. For example, the 2%Mo-2%B and 10%Mo-10%B modification exhibit a significant reduction to the depth and the width of wear tracks. It indicates an enhanced ability for Cu-Ni alloy to withstand surface damages caused by the sliding pin.
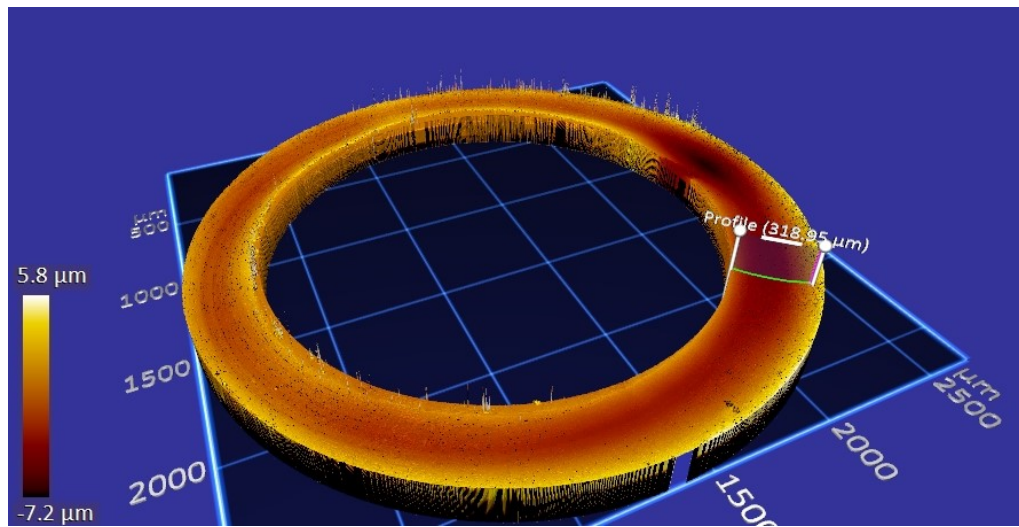
Figure 4. 6 Sliding wear track in air on 68Cu-32Ni with 2%Mo-2%B modification

Figure 4.6 shows the cross-sectional distance of the wear tracks. The diameter of spherical SiC sliders used for the wear test is 3 mm. Thus, based on the figure 4.2, β_0 can be estimated, since

$$\sin(\beta_0) = \frac{l}{2r}$$

The width of the wear track is demonstrated as *l*, and the radius of the spherical slider is listed as *r*. Profiles of the wear tracks show that all the widths of tracks are smaller than 400 μm. β_0, for all the wear tests after calculations, should be smaller than 7.6º, which is smaller than $\pi/2$. Thus, for all the cases of wear tests, the volume loss follows the same situation of (4.3) instead of a prismatic contact calculation. The volume loss can be compared under the same circumstance to reveal the intrinsic materials' wear resistance.
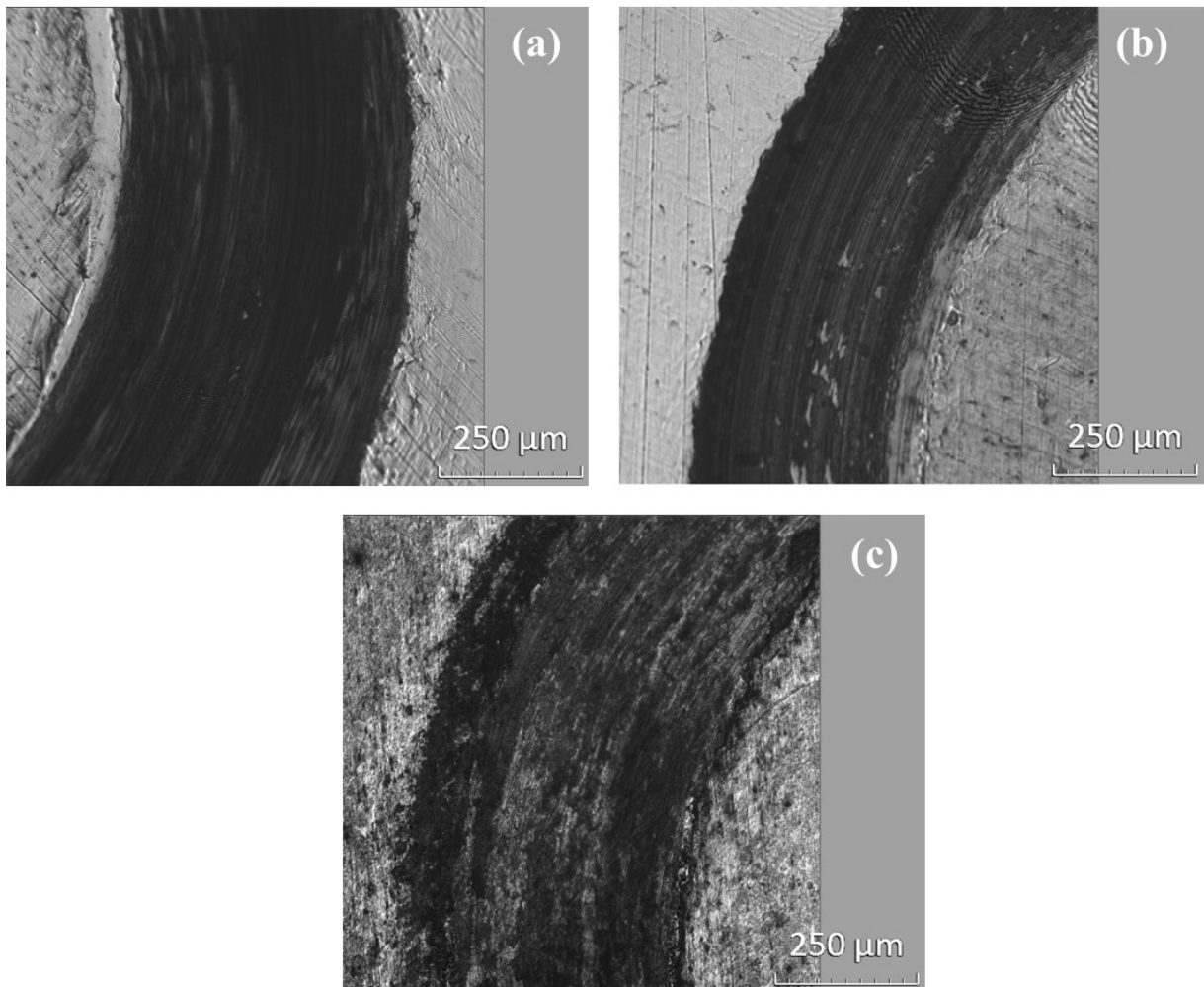
Figure 4. 7 Images of wear tracks in 3%NaCl solution (a) 68Cu-32Ni and (b) its with

2%Mo-2%B modification and (c) annealed low carbon steel

The images of wet wear tracks are displayed in figure 4.7. It is illustrated that in NaCl solution, Cu-Ni alloy has the widest wear track. Modified Cu-Ni alloys and steel exhibit better wear resistances to volume loss. It is also demonstrated that Cu-Ni based alloys has a good resistance to the NaCl solution and corrosion product is rarely observed.

Figures 4.8 (a) and (b) illustrate wear losses (volume losses) of the samples in air and in 3%NaCl solution, respectively. The sliding distance of the test in NaCl solution was three times that of the test in air, which led to the fact that wear tracks in NaCl solution were wider. As figure 4.8 (a) shown, the volume loss of 50Cu-50Ni was significantly reduced by the addition of Mo, B and a combination of B and Mo. The combination of B and Mo was much more effective, leading to the reduction of volume loss by about five times.

Figure 4.8(b) shows volume loss rates of the samples in the dilute NaCl solution. It should be indicated that the volume losses of the samples in the NaCl solution were caused by wear test over a sliding distance that was three times as long as that for the wear tests in air. The reason of using the longer sliding distance was due to the fact that wear of the Cu alloy samples in the dilute NaCl solution was smaller than that in air due to their anti-corrosion capability and the lubrication effect of the dilute NaCl solution, which is not a strong corrosive medium to Cu alloys.
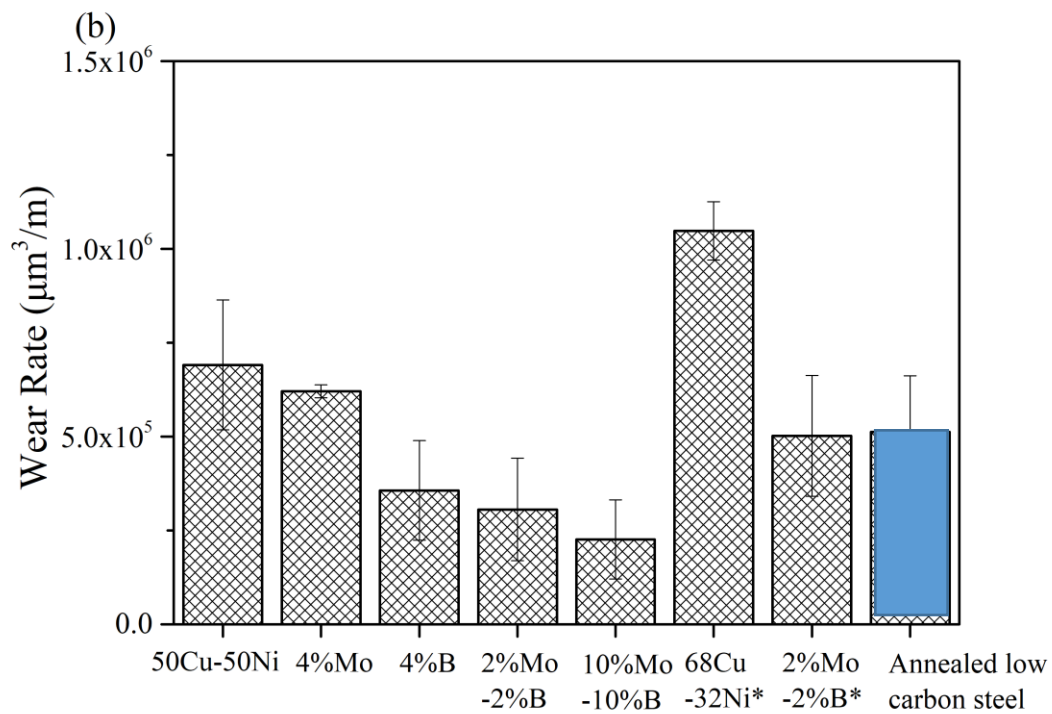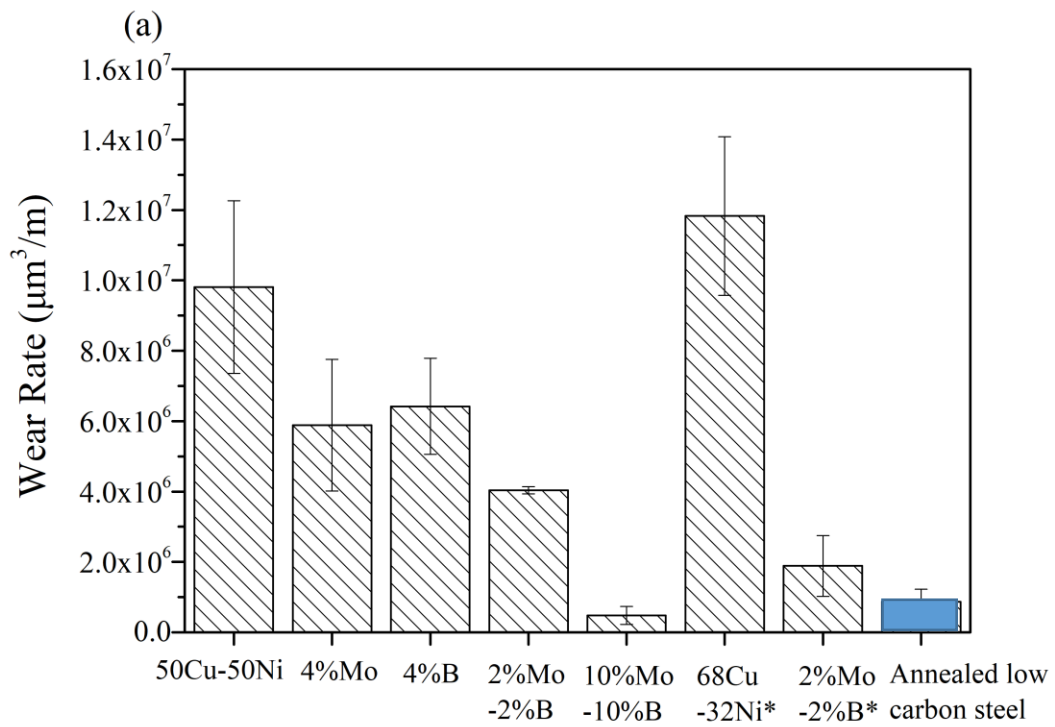
Figure 4. 8 Wear rates of samples (a) in air and (b) in a 3 wt.% NaCl solution.

As illustrated in figure 4.8, the influence of the alloying additions on corrosive wear of the Cu-Ni alloy is roughly similar to that under dry wear test condition. The wear resistance of the modified Cu alloys is considerably higher than that of the steel under both dry condition and in the dilute NaCl solution.

Corresponding coefficients of friction of the samples, which is the ratio of frictional force to the normal force, were also measured during the wear and corrosive wear tests, which are shown in figure 4.9. Under the dry wear condition, the addition of the alloying elements decreased the coefficient of friction and the combination of B and Mo was more effective in reducing the COF. The decreases in COF are consistent with those in wear loss, both of which are dependent on hardness of the materials. For COF, the higher the hardness, the smaller the contact area and thus the lower COF.

In the NaCl solution, the COFs of the samples are lower than those tested under dry condition due to the lubrication effect of dilute NaCl solution to the Cu alloy samples. As shown in figure 4.9 (b), after the initial increase, frictional coefficients of the samples in NaCl solution were in the range of 0.2 to 0.5. In comparison, the stable frictional coefficients in air were all above 0.5. The volume loss was reduced in the dilute NaCl solution. The COFs became stable after 250 seconds during the test in air while the COFs tend to continue increasing in the NaCl solution after 800 seconds. This could be ascribed to the continuous interaction between the worn surface and the corrosive solution. Debris from the surface wear was carried away by the solution and new film formed on the surface,

though was continuously destroyed by the wearing force. Again, the combination of B and Mo decreased the COF more than those of individual alloying elements. 10%Mo-10%B modified led to a significant decrease of the coefficient of friction. As measured, the COF of 50Cu-50Ni was reduced by 16% in air and 45% in NaCl solution. 2%Mo-2%B also showed strong effect on reduction in COFs of 70Cu-30Ni and 50Cu-50Ni.
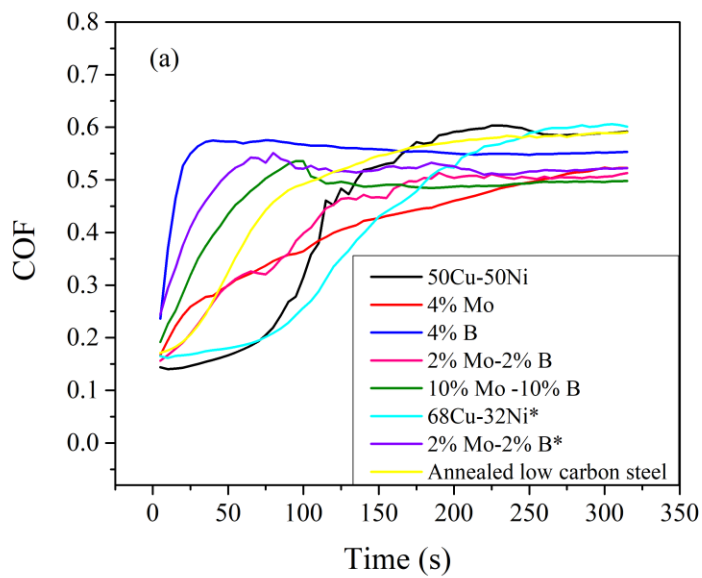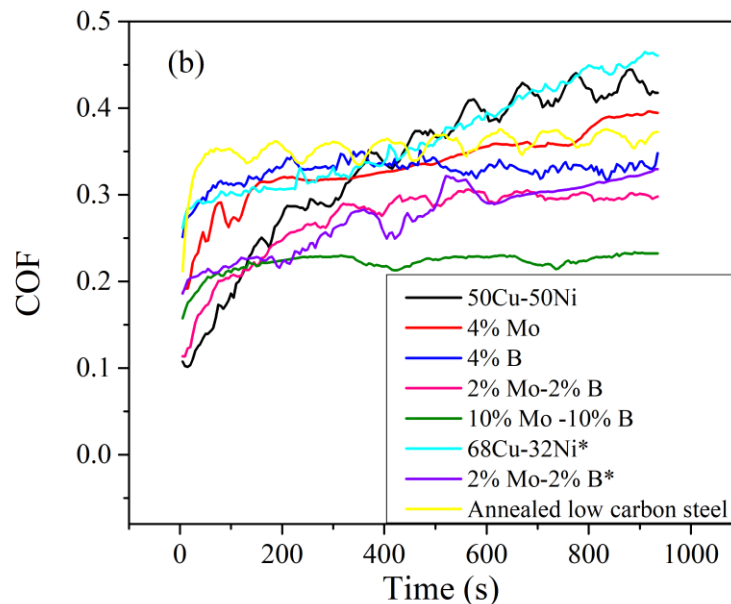
Figure 4. 9 Frictional coefficient of various samples (a) in air and (b) in 3 wt.% NaCl

solution.

The positive effects of Mo and B on the wear resistance and COF of the Cu-Ni alloy

are ascribed to the formation of second phases. B is more effective than Mo due to the

formation of borides which are generally hard and widely used in tool steel and many non-

ferrous alloys. The wear resistance of the alloy is closely related to the hardness of the

second phases. As stated previously, Vickers hardness of Ni_3B is 10490-10750 MPa and

hardness of Ni_4B_3 is 15690 MPa. The Vickers hardness of MoNi is 8924 MPa, which is

smaller than that of nickel borides by 15% to 43%. The presence of the Ni_3B or Ni_4B_3 phase

should be largely responsible for the increased mechanical strength of the original material

due to the fact that the nickel boride has high hardness and can result in exceptional wear

resistance [71-74].

The combination of Mo and B additives is more effective than a single additive to harden the alloy, leading to considerably elevated wear resistance. The effect could be ascribed to the formation of the solution hardening of the copper-nickel matrix, and the generation of more second phases as the XRD analysis shows. Regarding the solid hardening, Mo has its atomic radius (~140 pm [75]) larger than those of Ni (~125 pm [75]) and Cu (~128 pm [75]). This makes the solubility of Mo in the Cu-Ni alloy very low. B atom has a smaller atomic radius (~80 pm [75]). When Mo is added along B, the lattice distortion with compressive strain would be reduced, which favoring adding more Mo atoms. This helps enhance the solution hardening effect as more Mo can be accommodated by the CuNi alloy with lower strain energy when smaller B atoms co-exist. On the other hand, larger Mo atoms could also help more smaller B atoms dissolved in the CuNi matrix. These factors generate more barriers to dislocation motion, leading to increased mechanical strength and consequently higher wear resistance.

With increasing Mo and B additives, the wear resistance was further increased. As shown in figure 4.8, the volume loss of the 50Cu-50Ni alloy with, e.g., 2%B and 2%Mo, caused by wear was reduced by 59% and 56% when tested in air and 3% NaCl solution, respectively. The combination of 10%B and 10%Mo shows the most significantly enhanced wear resistance, corresponding to reduction of volume loss by 95% and 67% when tested in air and 3wt.% NaCl solution, respectively.

It should be stressed again that 10%B-10%Mo make the 50Cu-50Ni alloy stronger than the carbon steel in terms of the wear resistance in both air and the NaCl solution. This would widen the application range of the CuNi alloys.

4.4 Corrosion resistance

50Cu-50Ni alloy with 2%B-2%Mo and 10%Mo-10%B shows a higher hardness and much higher wear resistance than 50Cu-50Ni and the carbon steel as well. In order to evaluate how the addition of B and Mo influence its corrosion behavior, 50Cu-50Ni, and 50Cu-50Ni samples with 2%B-2%Mo and 10%B-10%Mo, 70Cu-30Ni and 70Cu-30Ni-2%B-2%Mo were tested with electrochemical polarization tests in 3wt.% NaCl solution to obtain their open circuit potentials and linear polarization resistance. Linear polarization resistance can be obtained by scanning a small range of voltage near the corrosion potential. The corrosion potential and the corresponding current are linear in the region, as shown in figure 4.10 (c). The constant slope of the potential and current curve refers to the polarization resistance, which gives the information of corrosion resistance of materials. In general, the higher the linear polarization resistance that a material has, the more resistant is the material to corrosion with a lower corrosion rate.

As shown in figure 4.10, the OCP measurement shows that 2%Mo and 2%B additives marginally lowered the open circuit potential of CuNi alloys. For example, the open circuit potential of 68Cu-32Ni was reduced by 0.024 V when 2%Mo-2%B were added,

corresponding to a relative decrease of 11% (see Table 4.1), suggesting that the additives do not influence much the tendency of the alloy to corrosion. Linear polarization resistance was obtained by fitting the linear region of the polarization curves to estimate corresponding corrosion resistance (Table 4.1). It is shown that 2%Mo and 2%B additives decreased the polarization resistance of the original Cu-Ni alloys more than the decrease in its OCP. For example, the polarization resistance of 50Cu-50Ni is decreased from 16690.4 to 7589.5 $\Omega\,cm^2$ by adding 2%Mo and 2%B, which should be ascribed to a higher corrosion current caused by the Mo and B addition. However, 10%Mo-10%B modified sample still shows a large polarization resistance of 13766.9 $\Omega\,cm^2$, relatively lower than that of 50Cu-50Ni but higher than that of 68Cu-32Ni alloy (8782.8 $\Omega\,cm^2$), suggesting a high corrosion resistance. Since this sample has a lower corrosion potential (OCP) as shown in Table 4.1, a higher linear polarization resistance implies that the corrosion current of this sample should be lower. Since the open circuit potential is measured without any applied potential or current, it is a measure of the thermodynamic tendency of a material to corrosion, while the polarization resistance is inversely proportional to the kinetic corrosion current. Thus, the corrosion rate of the 10%Mo-10%B is lower compared to other modified samples, although it has the lowest OCP.

The corrosion evaluation of low carbon steel was also added. Compared to CuNi and its modified alloys, steel has a much more negative open circuit potential -0.532 V, which is nearly 2 times the open circuit potential of CuNi alloy. Besides, the linear polarization resistance of steel, 1360 $\Omega\,cm^2$, is also relatively small. A more negative open circuit potential

and a smaller polarization resistance indicate an inferior corrosion resistance of steel to 3wt.% NaCl solution.

Table 4. 1- Linear polarization resistance (Rp) and open circuit potential (Eocp) of samples

Sample	Linear polarization resistance (Rp) / Ωcm^2	$Eocp(V_{SCE})$ /V
50Cu - 50Ni	16690.4	-0.210
2%Mo - 2%B	7589.5	-0.252
10%Mo – 10%B	13766.9	-0.285
68Cu - 32Ni*	8782.8	-0.218
2%Mo - 2%B*	3766.4	-0.242
Low carbon steel	1360.0	-0.532

(a)

(b)

(c)
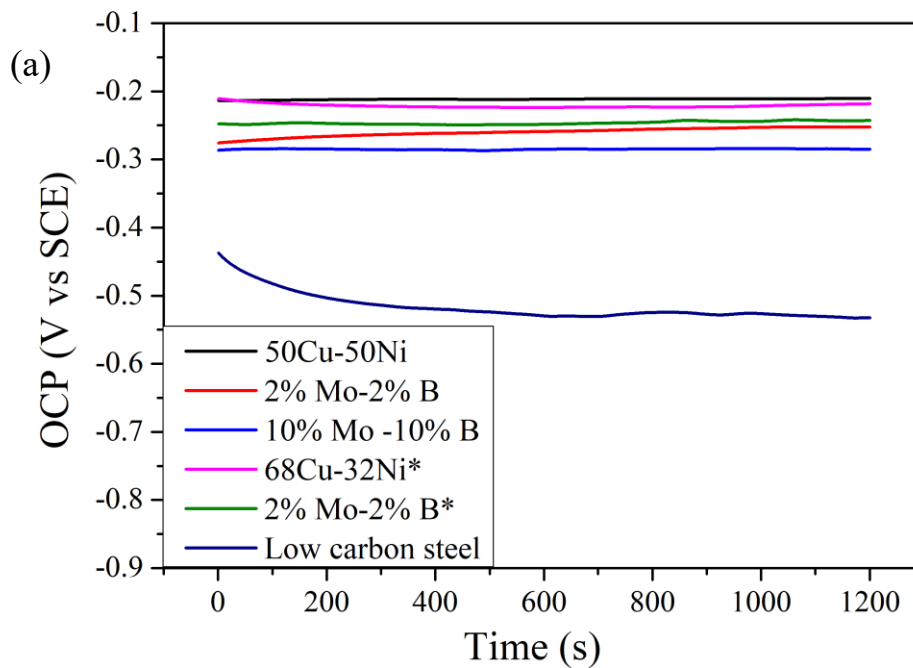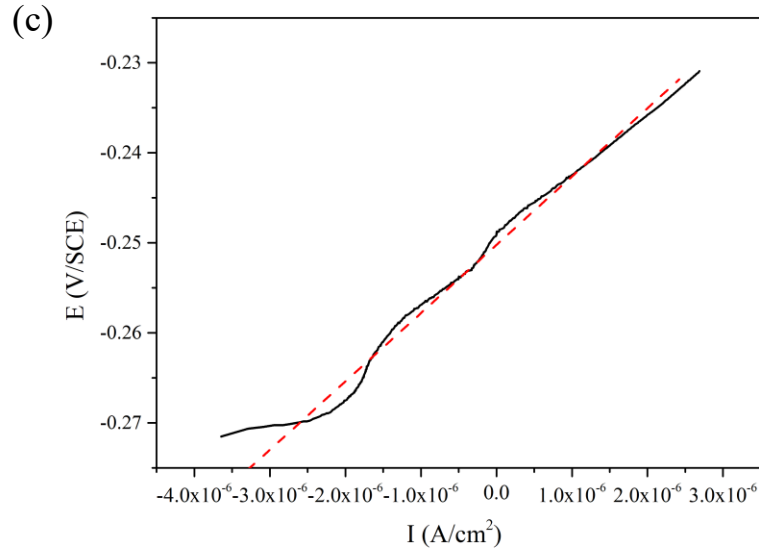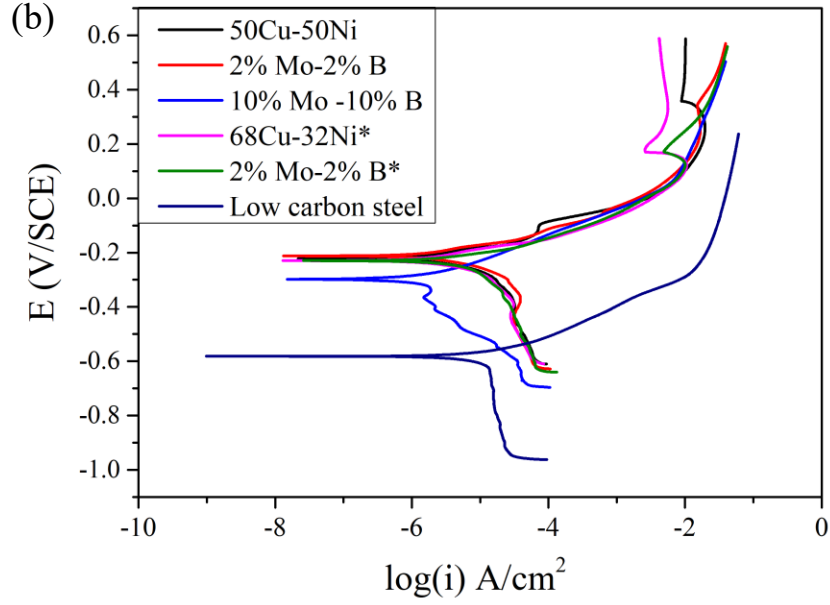
Figure 4. 10 (a) Open circuit potentials (b) polarization curves (c) red dashed

fitting line of the linear polarization curve of 50Cu-50Ni with 2%B-2%Mo modification

Figure 4.11 illustrates the possible mechanism for this result. Due to the generation of

second phases of bringing B and Mo to Cu-Ni alloy, preferential corrosion may occur and attack interphase boundaries of precipitation second phases. ZR Yang et al. [76] demonstrated the influence of the interphase boundaries on the corrosion behavior. It was found that the electron work function decreases at the interphase of TiC mircroparticles and Ni substrate. The process of corrosion refers to the loss of electrons of metal and the dissolution of materials into the corrosive media. Thus, a lower electron work function represents a worse corrosion resistance to the electrochemical reaction between the material and solution, which results into a lower open circuit potential. Since the electric conductivity of TiC is very low, the interphase is more anodic and a localized corrosion occurs between the interphase boundaries and Ni substrate.
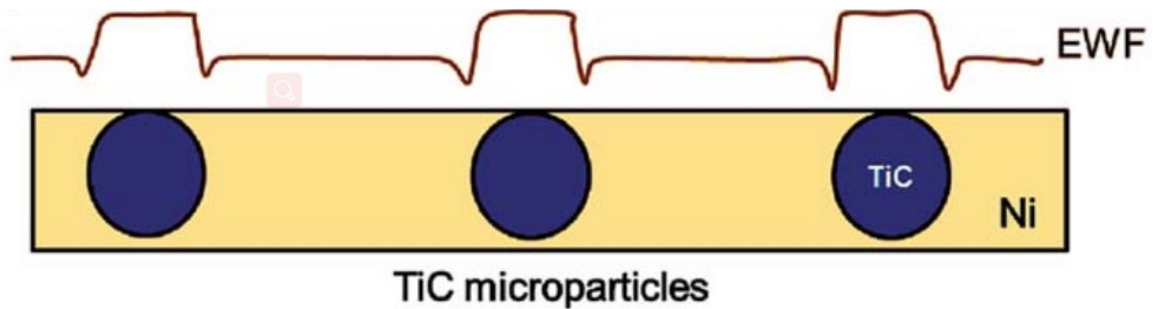
Figure 4. 11 Schematic of TiC microparticles in Ni matrix [76]

Similarly, the generated second phases of nickel borides have poor electric conductivity. For example, the conductivities of Ni_2B and Ni_3B are 0.07 S/m and 0.05 S/m [77], while the conductivity of Ni is $1.43×10^7$ S/m [78]. The interphase boundaries are

more anodic and thus create localized galvanic corrosion with the CuNi matrix. This could explain the rise of corrosion current after 2%Mo - 2%B modification. However, for 10%B-10%Mo, the precipitation phases of less conductive phases, such as phase Ni_3B, become more dominant over the materials surface. Thus, it restricts the current and mass exchange in these areas.

4.5 Further analysis on the strengthening effects of Mo and Boron

4.5.1 The strengthening effect Molybdenum

Mo alloys exhibit good wear and corrosion resistance [79]. Mo element can also be added to enhance the high-temperature resistance of alloys. It is assumed that Mo additive can strengthen the metal alloys by mechanisms of solid solution strengthening and precipitation hardening [80].

Solid solution strengthening

A small part of Mo can exist in Cu–Ni–Mo ternary alloys as solid solute atoms [81]. This contributes to the strengthening of the matrix phase CuNi. The Mo atom is larger than Cu and Ni atoms. When Mo atoms replace the original matrix atoms as substitutional solid solution, the local disorder due to the size misfit in the lattice generates a strain energy barrier to the dislocation motion. However, the solubility of Mo in CuNi binary continuous solid solution is quite small. The solid solubility of Mo in Cu is less than 4.3 at.% [82]. The

solubility of Mo in Ni is roughly 0.92 at.% in Ni at 300K based on the phase diagram. Thus It is believed that the effect of solid solution hardening by Mo is quite limited to the CuNi samples.

Precipitation hardening

Mo element mainly forms precipitation phases with Ni due to the strong interaction forces. Precipitation hardening is a very common method to strengthen metallic materials, such as steel, Al alloy and Cu alloy. The hardening is due to the finely dispersed second phases in the matrix phase. The interaction of these second phases impedes the movement of dislocation and enhance the alloys ability to withstand deformation. XRD analysis demonstrates the existence of MoNi and Mo_2NiB_5 second phases. For example, MoNi phase demonstrates a Vickers hardness of 8924 MPa. Meanwhile, the Vickers hardness of 50Cu-50Ni matrix is 833 MPa.

MoNi based alloys [83] have been extensively used as electrode materials due to its high electrochemical resistance. They can be used as anti-corrosion coatings in high corrosive acidic or basic environment due to their superb corrosion resistance. The alloys also demonstrate a good wear resistance as coating materials. E Chassaing et al. [84] investigated the corrosion resistance of MoNi alloy in 1M HCl solution. They fabricated MoNi alloy using electrochemical deposition on copper or iron plates. The Mo contents varied from 5 to 40 wt. % to compare the influence of the composition to the corrosion behavior. It was demonstrated that the corrosion resistance of MoNi alloy was directly

influenced by Mo content. The positivize effect of more Mo content on the intrinsic corrosion resistance of MoNi alloy contributes to an overall higher corrosion resistance. As shown in figure 4.12, the corrosion current density decreases with an increase of Mo composition.
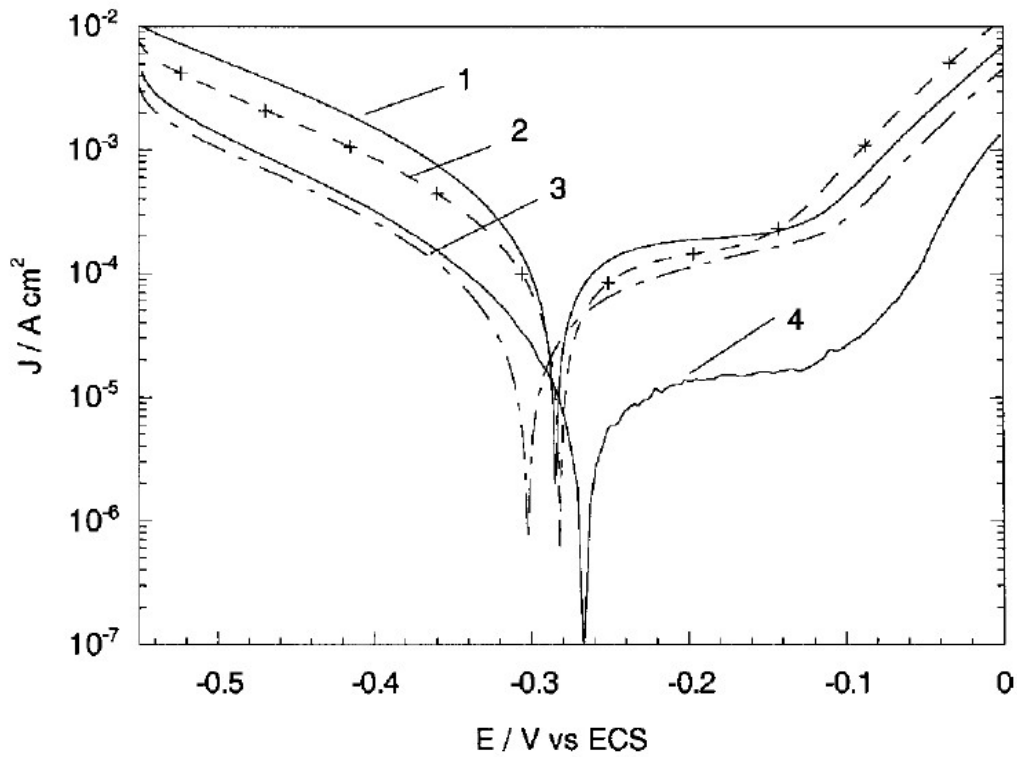
Figure 4. 12 Polarization curves of MoNi films [84]

However, the introduced MoNi phase also generated interphase boundaries in the CuNi matrix. These interphase boundaries become anodic and galvanic corrosion occurs. Thus, the addition of Mo content result into an increase of the corrosion current.

4.5.2 The strengthening of B

Solid solution strengthening

The similar effect of solid solution hardening applies to Boron additives. It was demonstrated that the solubility of Boron in copper is only 0.06 at.% at room temperature and 0.29 at. % at the eutectic temperature. Though the effect of boron additives to copper still needs further investigation. A. Y. Lozovoi et al [85] illustrated that boron atoms can strengthen the grain boundaries of copper. The boron atoms introduced to bulk copper form a strongly bound dimer and induce the disorder of lattice. In addition to copper, the solubility of boron in nickel is also quite low, which is about 0.15 at% to 0.3 at % [86] at the eutectic temperature. Thus, only a relatively small amount of boron atoms can form the solid solution with Cu-Ni alloy under the circumstances of 2% to 10 % boron addition. However, as previously discussed, relatively larger atoms of Mo and smaller atoms of B compared with Cu and Ni atoms, co-exist in the lattice and reduce the lattice distortion. This allows the accommodation of more solid solute atoms into the lattice and thus enhances the solution hardening effect, which could explain a better strengthening effect of 2 at.% B-2 at.% Mo modification than only 4 at.% B or 4 at.% Mo additives.

Precipitation hardening

Based on the phase diagram of B-Cu, no precipitation phase of Cu and B is observed. Thus the interaction of Cu and B is not further discussed here.

Ni and B can form a variety of nickel borides according to the B-Ni phase diagram. M.

Skibo et al [87] showed the strengthening effect of boron to nickel films fabricated through chemical vapor deposition. Boron was deposited in nickel with a composition from 0.0 wt.% to 0.2 wt. %. The microstructure analysis shows that a small amount of boron existed in the bulk nickel as interstitial atoms. The majority of boron additive atoms existed at the grain boundaries of nickel and formed discrete nickel boride particles. It was illustrated that boron content (up to 0.2 wt.%) increased the mechanical properties of nickel film by about 50%, including hardness and yield stress, which can be used as coatings for large load bearing applications.

The research of A. N. Campbell et al [86] also revealed the relationship between hardness and boron addition to nickel. Chemical vapor deposited Ni-B film was made. Ni_3B phases appeared after the anneal at 600 ºC and was verified by TEM images due to its different diffraction pattern. It was demonstrated that boron content greatly increases the materials hardness due to the precipitation hardening of Ni_3B phase. As illustrated in figure 4.13, the curve marked with ☐ represented the hardness of Ni-B sample with Ni_3B precipitation phase after annealing at 600 ºC for 1 hour. The Vickers hardness was increased from 200 to 690 due to the 5 at.% boron addition.
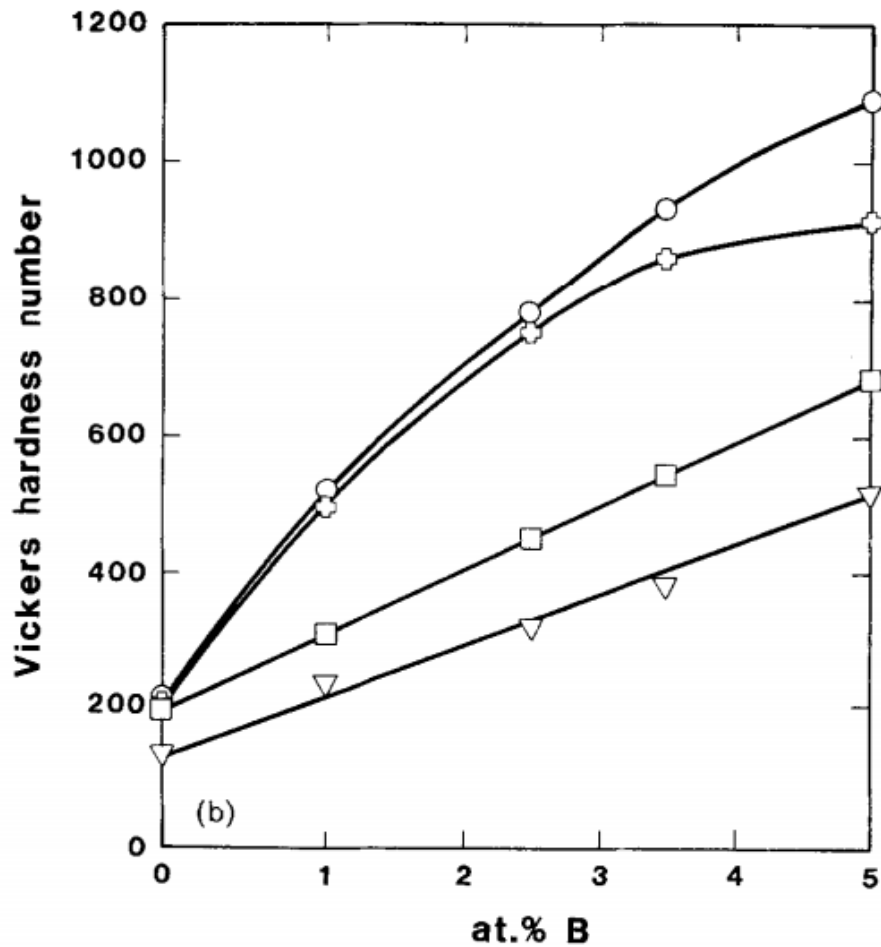
Figure 4. 13 Microhardness and the boron composition of Ni-B alloys [86]

The wear resistance of Ni-B has been studied as well [88]. It was found that the 13.0

at.% B alloyed nickel showed a precipitation phase of Ni_3B and exhibited high hardness

due to the precipitation hardening. For the wear test, pure nickel showed the ductile process

of smearing and tearing with an average wear track depth of 0.7 m under the normal load

of 50g. Compared to that, the wear appeared to be less ductile and the wear track was very

shallow for 13% B modified nickel with an average wear track depth smaller than 0.05 um under the normal load of 150g. Besides, the precipitation phase of Ni_3B showed a moderately low corrosion rate of 0.135 mm/y [89,90], measured in 3.5 wt. % NaCl solution. While the Cu-Ni alloy has a corrosion rate ranges from 0.025 to 0.0025 mm/y. This could explain the increased corrosion current from another perspective.

XRD analysis demonstrated the existence of Ni_3B and Mo_2NiB_5 phases in 50Cu-50Ni with 10%Mo-10%B addition, and Ni_4B_3 phase in 68Cu-32Ni with 2%Mo-2%B addition. The precipitation hardening of nickel borides greatly enhance the hardness and wear resistance.

4.5.3 The effect of microstructure on hardness and wear resistance

Based on Archard's wear equation, the wear performance of a material largely depends on its hardness. For heterogeneous materials, the wear rate is influenced by the combination of second phases and the matrix. As illustrated above, the addition of B and Mo introduced phases with higher hardness, such as MoNi (Vickers hardness: 8924 MPa) and Ni_4B_3 (Vickers hardness: 15690 MPa) phases, into the relatively softer CuNi alloy. The Vickers harnesses of 50Cu-50Ni is 833 MPa and 68Cu-32Ni is softer. The hard precipitation of second phases was added to the soft matrix to reinforce the Cu-Ni alloy, as illustrated in figure 4.14. Different factors can influence this reinforcement, such as the intrinsic

hardness, distribution, size and fraction of particles. Thus, with Mo and B elements added into the matrix, second phases with higher microhardness were introduced. The micro hardness of these second phases and the soft matrix contribute together to an overall high macro hardness of the material.
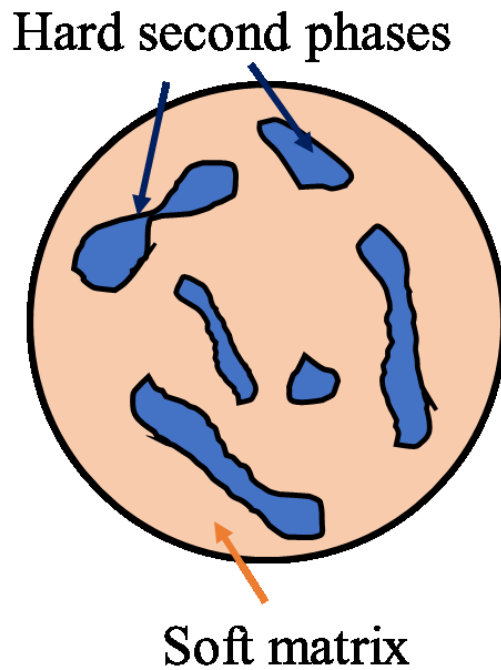
Figure 4. 14 Illustration of reinforcing phases

Chapter 5 Conclusions and Future Work

5.1 Conclusions

The copper-nickel alloy was modified by additives of molybdenum and boron. Effects of the additives and their combinations on hardness, resistances to wear and corrosive wear, and corrosion behavior of the Cu-Ni alloys were investigated.

1. It is demonstrated that the Mo and B additives result in significant increases in hardness. Compared with the 50Cu-50Ni sample, the hardness of the sample with 2 at.% B and 2 at.%. Mo addition was increased by 80%. Hardness of the modified Cu alloys can be higher than that of carbon steel (ASTM A109).

2. The resistances of the modified Cu-Ni alloys to wear and corrosive wear in air and in 3 wt.% NaCl solution, respectively, were considerably higher than those of unmodified Cu-Ni alloys; some of them performed better than the steel under study as well. The volume loss of the 50Cu-50Ni alloy with, e.g., 2 at.% B and 2 at.% Mo, caused by wear was reduced by 59% and 56% when tested in air and 3 wt.% NaCl solution, respectively. The combination of 10 at.% B and 10 at.% Mo shows the most significantly enhanced wear resistance, corresponding to reduction of volume loss by 95% and 67% when tested in air and 3wt.% NaCl solution, respectively.

3. The addition of 2%B and 2%Mo decreased the linear polarization resistance of the

CuNo alloys with marginally decreased corrosion potential (OCP) in the 3 wt. % NaCl solution. The addition of 10%Mo-10%B led to more decrease in OCP. However, the 10%B-10%Mo sample still shows a high polarization resistance, relatively lower than that of 50Cu-50Ni but higher than that of 68Cu-32Ni, which should be ascribed to a lower corrosion current or corrosion rate of this modified sample containing Mo and B of higher concentrations. Compared to the low-carbon steel, all the modified Cu-Ni samples possess considerably higher corrosion resistances.

4. The combination of Mo and B additives is more effective than a single additive in strengthening the Cu-Ni alloy.

5.2 Future work

1. The addition of Mo and B introduced various second phases. Since the interfacial boundaries are closely related to the corrosion resistance of materials, the properties of these interfaces can be further investigated. This may be done by collecting the electron work function data from these phases and the boundaries using atomic force microscopy, since electron work function can be an indicator of the state of electrons and the resistance to electrochemical reactions.

2. Different combinations of B and Mo additives have been investigated in the experiment, which show different wear and corrosion behaviors. However,

types and the amount of the additive elements can vary. Thus theoretical computational simulation can be performed to further understand and predict the microstructure and phase distribution under each circumstance.

3. All the samples were annealed at 600 ºC for 4 hours. This is a typical heat treatment for CuNi alloys. However, with Born and Mo addition, the microstructures become more complicated. For example, it is shown that the MoNi phase exists in the sample, which is not a thermodynamically favored phase at the room temperature based on the phase diagram of Mo-Ni. Thus, the effect of heat treatment on the precipitation strengthening of materials can be further investigated.

Bibliography

[1] Revie RW. Corrosion and corrosion control: an introduction to corrosion science and engineering. John Wiley & Sons; 2008 May 16.

[2] Koch G, Varney J, Thompson N, Moghissi O, Gould M, Payer J. International measures of prevention, application, and economics of corrosion technologies study. NACE International. 2016 Mar 1.

[3] Hansson CM. The impact of corrosion on society. Metallurgical and Materials Transactions A. 2011 Oct 1;42(10):2952-62.

[4] Ahmad, Zaki. Principles of Corrosion Engineering and Corrosion Control. Amsterdam: Elsevier/BH, 2006.

[5] Yepez, Omar. (2018). On the Mechanism of High Temperature Corrosion.

[6] François R, Laurens S, Deby F. Corrosion and Its Consequences for Reinforced Concrete Structures. Elsevier; 2018 Jan 16.

[7] Brunner G. Corrosion in Hydrothermal and Supercritical Water. InSupercritical Fluid Science and Technology 2014 Jan 1 (Vol. 5, pp. 591-619). Elsevier.

[8] S.Hiromoto, Corrosion of metallic biomaterials, Metals for Biomedical Devices, Woodhead Publishing Series in Biomaterials, 2010, Pages 99-121

[9] Vargel C. Corrosion of aluminium. Elsevier; 2004 Dec 30.

[10] Colvin EL., Aluminum Alloys: Corrosion, Encyclopedia of Materials: Science and Technology (Second Edition), 2001

[11] Gao J, Jiang Y, Deng B, Zhang W, Zhong C, Li J. Investigation of selective corrosion resistance of aged lean duplex stainless steel 2101 by non-destructive electrochemical techniques. Electrochimica Acta. 2009 Oct 1;54(24):5830-5.

[12] Popov BN. Corrosion engineering: principles and solved problems. Elsevier; 2015 Feb 26.

[13] Dennis A. Snow,   Plant Engineer's Reference Book, 2003

[14] Song GL, editor. Corrosion prevention of magnesium alloys. Elsevier; 2013 Feb 22.

[15] Kutz M. Handbook of environmental degradation of materials. William Andrew; 2018 Jun 15.

[16] Christodoulou C, Glass G, Webb J, Austin S, Goodier C. Assessing the long term benefits of Impressed Current Cathodic Protection. Corrosion Science. 2010 Aug 1;52(8):2671-9.

[17] Chess PM, Broomfield JP, editors. Cathodic protection of steel in concrete. CRC Press; 2003 Sep 2.

[18] Holmberg K, Erdemir A. Influence of tribology on global energy consumption, costs and emissions. Friction. 2017 Sep 1;5(3):263-84.

[19] Dong H, editor. Surface engineering of light alloys: aluminium, magnesium and titanium alloys. Elsevier; 2010 May 24.

[20] Neale MJ, editor. Lubrication and reliability handbook. Newnes; 2001 Jan 5.

[21] Tanzi MC, Farè S, Candiani G. Foundations of Biomaterials Engineering. Academic Press; 2019 Mar 16.

[22] Bloch HP, Geitner FK. Practical Machinery Management for Process Plants: Volume 2: Machinery Failure Analysis and Troubleshooting. Elsevier; 1997 Sep 11.

[23] Jiménez AE, Bermúdez MD. Friction and wear. InTribology for Engineers 2011 Jan 1 (pp. 33-63). Woodhead Publishing.

[24] Franc JP, Michel JM. Fundamentals of cavitation. Springer science & Business media; 2006 Jan 22.

[25] Alojali HM, Benyounis KY., Advances in Tool wear in Turning Process, Reference Module in Materials Science and Materials Engineering, Elsevier, 2016

[26] Doi T, Uhlmann E, Marinescu ID, editors. Handbook of ceramics grinding and polishing. William Andrew; 2015 Nov 19.

[27] Lindley,T.C. Fretting Fatigue, Encyclopedia of Materials: Science and Technology (Second Edition), 2001.

[28] Yusoff Z, Jamaludin SB. Tribology and Development of Wear Theory: Review and Discussion, 2011

[29] Sharma N, Alam SN, Ray BC, Yadav S, Biswas K. Wear behavior of silica and alumina-based nanocomposites reinforced with multi walled carbon nanotubes and graphene nanoplatelets. Wear. 2019 Jan 15;418:290-304.

[30] Hutchings I, Shipway P. Tribology: friction and wear of engineering materials. Butterworth-Heinemann; 2017 Apr 13.

[31] Dossett J, Totten GE. Introduction to surface hardening of steels. ASM Handbook. 2013;4:389-98.

[32] Ma GZ, Xu BS, Wang HD, Li GL, Zhang S. The low-temperature ion sulfurizing technology and its applications. Physics Procedia. 2013 Jan 1;50:131-8.

[33] Najmie A. Abrasion and erosion wear properties of surface deformed stainless steel, June 2016.

[34]Ganesh BK, Sha W, Ramanaiah N, Krishnaiah A. Effect of shotpeening on sliding wear and tensile behavior of titanium implant alloys. Materials & Design (1980-2015). 2014 Apr 1;56:480-6.

[35] Inwood BC, Garwood AE. Electroplated coatings for wear resistance. Tribology international. 1978 Apr 1;11(2):113-9.

[36] Morre MA. The abrasive wear resistance of surface coatings. Journal of Agricultural Engineering Research. 1975 Jun 1;20(2):167-79.

[37] Luiz Otávio Amaral Affonso, 6 – Wear, Machinery Failure Analysis Handbook, Gulf Publishing Company, Pages 55-82, 2006.

[38] B. Phull. Marine Corrosion. Shreir's Corrosion, 1107-1148; 2010.

[39] Todd B. Marine Applications of Copper–Nickel Alloys, Section 2: Materials Selection for High Reliability Seawater Systems. InTechnical Report 1998. Copper Development Association Potters Bar, UK.

[40] Francis R. Copper Alloys in Seawater: Avoidance of Corrosion. Copper Development Association; 2016.

[41] Al-Hajji JN, Reda MR. Corrosion of Cu-Ni alloys in sulfide-polluted seawater. Corrosion; 1993 Oct;49(10):809-20.

[42] Kear G, Barker BD, Stokes K, Walsh FC. Electrochemical corrosion behaviour of 90—10 Cu—Ni alloy in chloride-based electrolytes. Journal of Applied Electrochemistry. 2004 Jul 1;34(7):659-69.

[43] Francis R. The Corrosion of Copper and Its Alloys: A Practical Guide for Engineers. NACE International; 2010.

[44] Copper and Copper Alloy Castings - Properties and Applications, Copper Development Association; 1991.

[45] Hughes SE. Materials and Their Weldability. In A Quick Guide to Welding and Weld Inspection 2009. ASME Press.

[46] North RF, Pryor MJ. The influence of corrosion product structure on the corrosion rate of Cu-Ni alloys. Corrosion Science. 1970 Jan 1;10(5):297-311.

[47] Sahoo, M. Sahu, S. Whiting, L. V. Sadayappan, K.. Casting Copper-Base Alloys (3rd Edition). American Foundry Society; 2015.

[48] Robert H. Thurston and Burndy Library, A Treatise on Brasses, Bronzes, and Other Alloys, and Their Constituent Metals. Materials of Engineering, 2 ed., 1890. 589 pp.

[49] Benvenuto MA. Metals and Alloys: Industrial Applications. Walter de Gruyter GmbH & Co KG; 2016.

[50] Gohn GR. The mechanical properties of copper-beryllium alloy strip. ASTM International; 1964.

[51] Huang XC, Lu H, Li DY. Understanding the corrosion behavior of isomorphous Cu–Ni alloy from its electron work function. Materials Chemistry and Physics. 2016 Apr 15;173:238-45.

[52] Davis JR, editor. Surface engineering for corrosion and wear resistance. ASM international; 2001. [15] Zum Gahr KH. Microstructure and wear of materials. Elsevier; 1987.

[53] Divakar R, Blau P. Wear testing of advanced materials. ASTM International; 1992.

[54] Yin S, Li DY, Bouchard R. Effects of the strain rate of prior deformation on the wear–corrosion synergy of carbon steel. Wear. 2007 Sep 10;263(1-6):801-7.

[55] Ibbotson, F. The Analysis of Non-ferrous Alloys. Ed.2 London: Longmans, 1922.

[56] Askeland D.R. Ferrous Alloys. In: The Science and Engineering of Materials. Springer; 1996.

[57] Azarkevich, A.A., Kovalenko, L.V. & Krasnopolskii, V.M. Met Sci Heat Treat. 1995; 37: 22.

[58] Weber,J.H., Fahrman,M.G., Crum,J.R., Nickel: Alloying, 2001, 6135-6140, Elsevier, Oxford.

[59] Finch CB, Cavin OB, Becher PF. Crystal growth and properties of trinickel boride, Ni3B. Journal of crystal growth. 1984 Aug 1;67(3):556-8.

[60] Berlin J. Analysis of boron with energy dispersive X-ray spectrometry. Imaging & Microscopy. 2011 May;13(2):19-21.

[61] Uruga K, Sawada K, Enokida Y, Yamamoto I. Liquid metal extraction for removal of molybdenum from molten glass containing simulated nuclear waste elements. Journal of nuclear science and technology. 2008 Oct 1;45(10):1063-71.

[62] Okamoto H, Schlesinger ME, Mueller EM. ASM Handbook, vol. 3. Alloy Phase Diagrams, ASM, Ohio. 2016.

[63] Samsonov GV. Mechanical properties of the elements. Handbook of the Physicochemical Properties of the Elements 1968 (pp. 387-446). Springer, Boston, MA.

[64] Molecular Hardness by material Kenneth Nordtvedt Molecular Hardness

[65] Motojima S, Maeda K, Sugiyama K. The boronization of nickel plate and some of its properties. Journal of the Less Common Metals. 1981 Oct 1;81(2):267-72.

[66] Song C, Wang S, Gui Y, Cheng Z, Ni G. Microstructure and Tribological Properties of Mo–40Ni–13Si.

[67] Huang XC, Lu H, He HB, Yan XG, Li DY. Correlation between the wear resistance of Cu-Ni alloy and its electron work function. Philosophical Magazine. 2015 Dec 2;95(34):3896-909.

[68] CRC Handbook of Chemistry and Physics version 2008, p. 12–114.Multiphase Intermetallic Alloy. Materials. 2016;9(12):986.

[69] Preston, F. W. Theory and design of glass polishing machines. J. Soc. Glass Technol., 1927, 11, 214–256.

[70] Kauzlarich JJ, Williams JA. Archard wear and component geometry. Proceedings of the Institution of Mechanical Engineers, Part J: Journal of Engineering Tribology. 2001 Apr 1;215(4):387-403.

[71] Campos-Silva I, Contla-Pacheco AD, Figueroa-López U, Martínez-Trinidad J, Garduño-Alva A, Ortega-Avilés M. Sliding wear resistance of nickel boride layers on an Inconel 718 superalloy. Surface and Coatings Technology. 2019 Aug 5:124862.

[72] Oraon B, Majumdar G, Ghosh B. Improving hardness of electroless Ni–B coatings using optimized deposition conditions and annealing. Materials & design. 2008 Jan 1;29(7):1412-8.

[73] Ivanov MV. Electroless nickel–boron–phosphorus coatings: protective and functional properties. Protection of Metals. 2001 Nov 1;37(6):592-6.

[74] Delaunois F, Petitjean JP, Lienard P, Jacob-Duliere M. Autocatalytic electroless nickel-boron plating on light alloys. Surface and Coatings Technology. 2000 Feb 21;124(2-3):201-9.

[75] Smith DW. Inorganic substances: a prelude to the study of descriptive inorganic chemistry. Cambridge university press; 1990 Jan 18.

[76] Yang Z, Lu H, Liu Z, Yan X, Li D. Effect of particle size on the surface activity of TiC–Ni composite coating via the interfacial valence electron localization. RSC Advances. 2016;6(23):18793-9.

[77] Smolin MD, Grebenkina VG, Goryachev YM, Panov LI, Shvartsman EI. Electrophysical properties of nickel boride phases. Soviet Powder Metallurgy and Metal Ceramics. 1982 Aug 1;21(8):662-5.

[78] MatWeb LL. MatWeb—Material property data. Tra-Con Tra-Bond. 2013;2115.

[79] Li X, Liu Z, Wang Y. Microstructure and corrosion properties of laser cladding MoNi based alloy coatings. Science China Technological Sciences. 2014 May 1;57(5):980-9.

[80] De Luca A, Seidman DN, Dunand DC. Effects of Mo and Mn microadditions on strengthening and over-aging resistance of nanoprecipitation-strengthened Al-Zr-Sc-Er-Si alloys. Acta Materialia. 2019 Feb 15;165:1-4.

[81] Cheng X, Zhang Y, Li X, Li Z, Yu Q, Zheng Y, Wang C, Dong C. Microstructure evolution and strengthening mechanism of Cu x [Ni3Mo] alloys. Materials Science and Technology. 2019 Jan 2;35(1):98-106.

[82] Xi S, Zuo K, Li X, Ran G, Zhou J. Study on the solid solubility extension of Mo in Cu by mechanical alloying Cu with amorphous Cr (Mo). Acta Materialia. 2008 Dec 1;56(20):6050-60.

[83] Athanassiou EK, Grass RN, Osterwalder N, Stark WJ. Preparation of homogeneous, bulk nanocrystalline Ni/Mo alloys with tripled vickers hardness using flame-made metal nanoparticles. Chemistry of Materials. 2007 Oct 2;19(20):4847-54.

[84] Chassaing E, Portail N, Levy AF, Wang G. Characterisation of electrodeposited nanocrystalline Ni–Mo alloys. Journal of Applied Electrochemistry. 2004 Nov 1;34(11):1085-91.

[85] Lozovoi AY, Paxton AT. Boron in copper: A perfect misfit in the bulk and cohesion enhancer at a grain boundary. Physical Review B. 2008 Apr 10;77(16):165413.

[86] Campbell AN, Mullendore AW, Hills CR, Vandersande JB. The effect of boron on the microstructure and physical properties of chemically vapour deposited nickel films. Journal of materials science. 1988 Nov 1;23(11):4049-58.

[87] Skibo M, Greulich FA. Characterization of chemically vapor deposited Ni-(0.05-0.20 wt.%) B alloys. Thin solid films. 1984 Mar 23;113(3):225-34.

[88] Mullendore AW, Pope LE. Wear resistance of metastable Ni-B alloys produced by chemical vapor deposition. Thin solid films. 1987 Oct 26;153(1-3):267-79.

[89] Dervos CT, Novakovic J, Vassiliou P. Vacuum heat treatment of electroless Ni–B coatings. Materials Letters. 2004 Feb 1;58(5):619-23.

[90] Riddle YW, Bailerare TO. Friction and wear reduction via an Ni-B electroless bath coating for metal alloys. Jom. 2005 Apr 1;57(4):40-5.